Pairing $\Delta N_2/Ar$ and N* tracers to observe denitrification in the Canada Basin

by

Jennifer L. Reeve

B.Sc., Haverford College, 2014

A Thesis Submitted in Partial Fulfillment of the

Requirements for the Degree of

MASTER OF SCIENCE

in the School of Earth and Ocean Sciences

Pairing $\Delta N_2/Ar$ and N* tracers to observe denitrification in the Canada Basin

by

Jennifer L. Reeve

B.Sc., Haverford College, 2014

Supervisory Committee

---

Dr. Roberta Hamme, Supervisor

(School of Earth and Ocean Sciences)

---

Dr. Jay Cullen, Departmental Member

(School of Earth and Ocean Sciences)

---

Dr. Thomas Pedersen, Departmental Member

(School of Earth and Ocean Sciences)

---

Dr. William Williams, Outside Member

(Institute of Ocean Sciences)

**Supervisory Committee**

---

Dr. Roberta Hamme, Supervisor

(School of Earth and Ocean Sciences)

---

Dr. Jay Cullen, Departmental Member

(School of Earth and Ocean Sciences)

---

Dr. Thomas Pedersen, Departmental Member

(School of Earth and Ocean Sciences)

---

Dr. William Williams, Outside Member

(Institute of Ocean Sciences)

## ABSTRACT

Our understanding of the global marine fixed nitrogen budget has undergone rapid growth, and as a result there is debate as to whether or not it is balanced. The Arctic plays a disproportionately large role in the sink terms of this budget. This paper works to understand the role of the Canada Basin in the nitrogen cycle. We utilize two tracers of denitrification: $N_2$/Ar, a dissolved gas tracer, and N*, a nutrient ratio tracer. We aim to quantify the current state of nitrogen cycling in the Canada

Basin, and determine its role in the global cycle. Our paired tracer method provides support for shelf denitrification rates while providing an estimate of ventilation in the same water mass, and provides an estimate for deep benthic denitrification rates. We observe a disconnect between $N_2$/Ar and N* in the Pacific Upper Halocline Layer (PUHL), wherein the excess $N_2$/Ar we expect from N* is nearly 250% larger than the excess we observe. Our calculations suggest that an approximate steady state between benthic denitrification and gas exchange on the Chukchi shelf maintains this disconnect. Our measurements of the PUHL support the shelf denitrification rates reported from direct measurements, and can predict wind speeds required for ventilation within a factor of two. A 1D diffusion model of the old deep waters of the Canada Basin supports benthic denitrification rates of 0.095-0.15 Tg N $y^{-1}$. Benthic denitrification rates determined from the model are on the low end of rates in other deep basins. Our results suggest additional measurements of these tracers in the Canada Basin and surrounding areas would help to constrain both the physical and biological processes controlling nitrogen cycling.

# Contents

# List of Tables

# List of Figures

# ACKNOWLEDGEMENTS

I would like to thank:

**Roberta Hamme,** for guidance, an introduction to modeling, debugging help, and lots of edits.

**my wonderful housemates,** for a lot of laughter and stress relief through marking lab reports and late nights in the lab.

**the scientific and Coast Guard crew of the JOIS 2015 research cruise,** for a wonderful welcome to oceanographic research cruises, and a month of sea ice, polar bears and adventure.

**my labmates and the rest of the SEOS graduate students,** for the constant reminder to enjoy life and do research, and help in doing both tasks.

**The University of Victoria,** for a beautiful campus, an education, and funding my research.

**Mark Altabet,** for his suggestions and guidance as my external examiner.

**NSERC: Climate Change and Atmospheric Research (CCAR): The Canadian Arctic GEOTRACES Program: Biogeochemical and tracer study of a rapidly changing Arctic and NSERC CCAR: Ventilation, Interactions and Transports Across the Labrador Sea (VITALS),** for funding my research.

# Chapter 1

# Introduction

The marine nitrogen cycle is one of the largest controls on ocean productivity. Changes in the global marine bioavailable nitrogen inventory are thought to have driven changes in global ocean productivity rates that in turn may have been partially responsible for glacial-interglacial atmospheric $CO_2$ variations [*McElroy*, 1983; *Altabet et al.*, 1999, 2002; *Liu et al.*, 2005; *Galbraith et al.*, 2013]. To understand how the biological carbon pump will respond to climate change, we need to quantify the various processes of the marine nitrogen cycle and understand their controls.

While the most abundant form of nitrogen is $N_2$ gas, it is inaccessible to most life. To be used for growth, $N_2$ has to undergo nitrogen fixation, performed by a small class of marine organisms called diazotrophs. Bioavailable forms of nitrogen are called fixed nitrogen, and include nitrate, nitrite, ammonium, and organic nitrogen among others. The marine nitrogen budget is dominated by the source and sink terms for fixed nitrogen. Fixed nitrogen is removed by a set of processes which convert it back into $N_2$ gas. Canonical denitrification converts $NO_3$ to $N_2$ through a series of heterotrophic reactions, and anammox converts ammonium and nitrite to $N_2$ as an autotrophic process. We will refer to all processes that convert fixed nitrogen to $N_2$ as

denitrification. Denitrification is a predominantly anoxic process and, as such, occurs primarily in oxygen deficient waters and sediments. Recent research has resulted in larger estimates both of global nitrogen fixation sources and of denitrification sinks, with estimates denitrification rates moving from 120 Tg N $y^{-1}$ [*Codispoti and Christensen*, 1985] to conservatively upwards of 200 Tg N $y^{-1}$ [*Bianchi et al.*, 2012; *DeVries et al.*, 2013] with some estimates above 400 Tg N $y^{-1}$ [*Codispoti*, 2007]. As a result, different assumptions about the controls on these processes have resulted in estimates for the global marine nitrogen budget with significant fixed nitrogen deficits [*Middelburg et al.*, 1996; *Codispoti*, 2007], as well as estimates with relatively balanced sources and sinks of fixed nitrogen [*Gruber and Sarmiento*, 1997; *Gruber*, 2004; *Bianchi et al.*, 2012; *DeVries et al.*, 2013].

Despite the lack of oxygen deficient water, the Arctic makes significant contributions to the global denitrification rate [*Middelburg et al.*, 1996; *Devol et al.*, 1997; *Chang and Devol*, 2009; *Bianchi et al.*, 2012; *DeVries et al.*, 2013; *McTigue et al.*, 2016], due to a relatively high proportion of the global continental shelf area. Measurements of nitrogen cycle rates in the Arctic are largely limited to the Bering and Chukchi shelves. In addition to significant contributions to the global denitrification rate, there have been some measurements to suggest that the Arctic, and Canadian Arctic specifically, contributes to the global nitrogen fixation rate as well [*Blais et al.*, 2012].

The Arctic is undergoing rapid changes due largely to anthropogenic climate change, with decreasing ice cover and increasing temperatures and stratification [*Grebmeier et al.*, 2010; *Tremblay et al.*, 2012; *Vaughan et al.*, 2013; *Kirtman et al.*, 2013; *Steiner*, 2015]. Every measure of sea ice in the Arctic has undergone decreases dating back at least as far as satellite measurements are available [*Vaughan et al.*, 2013]. In the region stretching from the East Siberian Sea to the western

Canada Basin the summer ice free period increased by three months from 1979 to 2011 [*Vaughan et al.*, 2013], with most models predicting an ice free summer by the end of the century at the latest [*Kirtman et al.*, 2013]. While our models are increasingly able to predict changes in sea ice, the net effect of these physical changes on Arctic ecosystems is ill constrained [*Grebmeier et al.*, 2010]. Some estimates show greatly increased net primary production in the Arctic Ocean due to decreased sea ice cover [*Grebmeier et al.*, 2010; *Larsen et al.*, 2014]; however, these increases are not unilaterally supported by the data available [*Grebmeier et al.*, 2010]. The lack of accessibility to the region during significant portions of the year has not aided in our ability to understand the controls on both physical and biological processes occurring in the Arctic. The Bering and Chukchi Shelves are known to have high rates of denitrification [*Devol et al.*, 1997; *Tanaka et al.*, 2004; *Yamamoto-Kawai et al.*, 2006; *Chang and Devol*, 2009; *Granger et al.*, 2011; *Souza et al.*, 2014; *Brown et al.*, 2015; *McTigue et al.*, 2016], and it is important that we understand the controls on and rates of nitrogen processes in order to understand the global nitrogen cycle.

This thesis focuses on the Canada Basin (Figure 1.1) in the Amerasian portion of the Arctic Ocean. Water flowing from the Pacific generally follows three pathways once leaving the Chukchi Shelf: in the first, water flows along the Beaufort Shelf and into the Canadian Arctic Archipelago via the Amundsen Gulf, in the second, water flows north of the Canada Basin, and in the third, water flows into the Canada Basin and Beaufort Gyre. Pacific water in the Canada Basin lies below a layer of fresh cold melt water, and above the Atlantic origin water masses. We sampled full depth profiles in the Canada Basin and present data from all water masses; however, in-depth discussion in this thesis focuses on the core of the Pacific water layer and the deepest water in the Canada Basin.

To trace signals of denitrification off the Chukchi Shelf into the Canada Basin,

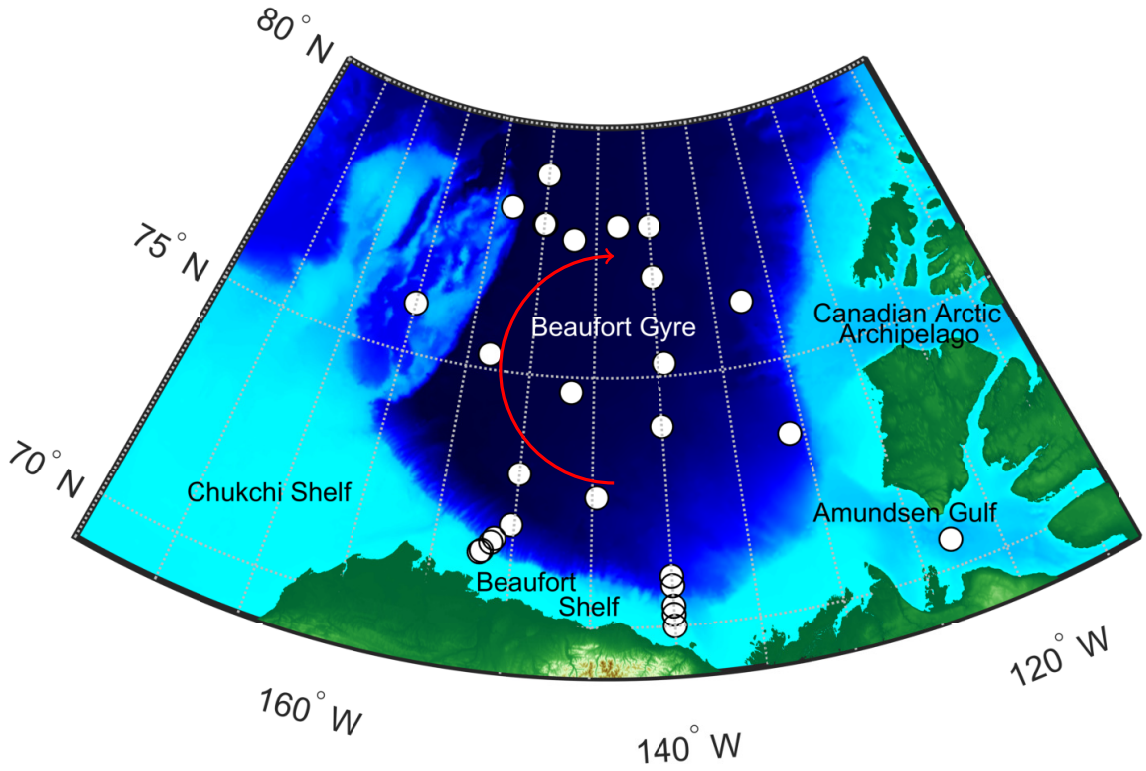


**Figure 1.1: Map of the Canada Basin and surrounding areas** with locations of $N_2$/Ar sampling during JOIS 2015. Water depth is indicated by color, with darker blues indicating deeper water. The red arrow indicates the movement of the Beaufort Gyre.

we combine two tracers of the marine nitrogen cycle: $N_2$/Ar, a dissolved gas tracer, and N*, a nutrient tracer. These tracers focus on different sides of the denitrification reaction ($2NO_3^- + 10e^- + 12H^+ \rightarrow N_2 + 6H_2O$). $N_2$/Ar measures the product of denitrification, while N* traces the reactant.

$N_2$/Ar acts as a tracer of biological inputs of $N_2$ gas due to denitrification. $N_2$/Ar has been used to quantify denitrification occurring in oxygen minimum zones [*Chang et al.*, 2010; *Bourbonnais et al.*, 2015] and the deep ocean [*Hamme and Emerson*, 2013; *Shigemitsu et al.*, 2016], as well as to measure benthic denitrification in sediment cores [*Chang and Devol*, 2009]. The tracer relies on the similar responses of $N_2$ and Ar to physical processes to allow observation of the effects of predominantly biotic processes on $N_2$. $N_2$/Ar is not believed to be a useful tracer of nitrogen fixation [*Shigemitsu et al.*, 2016].

Much of the world's oceans are characterized by a strong relationship between nitrate and phosphate which falls near a Redfieldian 16 to 1 ratio. N* measures deviations off of this ratio to determine if there is a relative deficit or surplus of nitrate. This tracer has evolved since its creation through several definitions. The initial definition of N* from *Gruber and Sarmiento* [1997] was $N* = ([NO_3] - 16[PO_4] + 2.90) * 0.87$, which set the global mean N* to be zero. One common variant includes more fixed nitrogen species than just nitrate, as in *Nishino et al.* [2005]; *Granger et al.* [2011]; *Mills et al.* [2015], this is used when other inorganic nitrogen species are likely to accumulate in the water column. We utilize the definition most commonly used in more recent literature [*Weber and Deutsch*, 2010; *Deutsch and Weber*, 2012] of $N* = [NO_3] - 16[PO_4]$, which makes no effort to set the intercept resulting in a slightly negative global mean. We did not utilize additional forms of fixed inorganic nitrogen because these water masses are oxygenated, and nitrification converts all inorganic fixed nitrogen into nitrate. N*, like $N_2$/Ar, has been put to use investigating

nitrogen cycling in many ways. N* is an easy to measure tracer with a global dataset which has made it useful to confirm model outputs [*DeVries et al.*, 2013], as well as to trace large scale trends in the marine nitrogen cycle [*Gruber and Sarmiento*, 1997; *Gruber*, 2004; *Deutsch and Weber*, 2012]. Nutrient ratios often used in the Arctic as a tracer of water masses due to the large differences in the N* value of incoming Pacific and Atlantic water [*Jones et al.*, 2003; *Codispoti et al.*, 2005; *Yamamoto-Kawai et al.*, 2006].

In addition to their different approaches to the question, these two methods make an informative combination because they are each sensitive to a different set of biases. $N_2$/Ar is sensitive to physical processes which affect $N_2$ and Ar differently [*Hamme and Emerson*, 2013]; whereas, N* is sensitive to variations in the N:P utilization ratios of phytoplankton [*Deutsch and Weber*, 2012].

The primary processes which affect $N_2$ and Ar dissolution in seawater differently are bubble injection and rapid cooling [*Hamme and Emerson*, 2002, 2013]. Injection of air into the water, by way of bubbles, increases the $N_2$ concentration disproportionately because it is less soluble than Ar in seawater [*Hamme and Emerson*, 2013]. Glacial ice shelves can also inject bubbles when melting, while sea ice captures $N_2$ in bubbles when forming, and releases these high $N_2$ bubbles upon melting, some but not all of which redissolve [*Hamme and Emerson*, 2002]. Rapid cooling affects $N_2$ and Ar differently due to differences in the temperature dependence of their solubilities. However, rapid cooling has a very small effect on the $N_2$/Ar ratio, and is unlikely to cause large variations in the ratio in the ocean [*Hamme and Emerson*, 2013].

Of importance for N* are the N:P ratios in organic matter which, while generally falling near the 16:1 canonical value, can be as wide ranging as 5 to 33.5 [*Deutsch and Weber*, 2012]. In euphotic waters, these variable ratios can alter the N* signature of the remaining water column nutrients, and in deeper waters can alter N* through

remineralization of organic matter with non-canonical N:P ratios. Low N:P uptake ratios increase the N* of remaining nutrients and decrease the N* of deeper waters upon remineralization, whereas high N:P ratios have the opposite effects. Additionally N* can be affected by changes in the rate of burial of phosphorus as organic matter, minerals, or adsorbed onto particles [*Ingall and Jahnke*, 1994; *Paytan and McLaughlin*, 2007]. One of the primary controls on phosphorus burial is bottom oxygen concentrations, with low bottom oxygen conditions enhancing phosphorus remineralization and decreasing burial and high bottom oxygen conditions enhancing phosphorus burial [*Ingall and Jahnke*, 1994; *Paytan and McLaughlin*, 2007].

Since denitrification only occurs in anoxic waters and the water column in our study area has reasonably high oxygen levels, the denitrification signal we expect to see in this region diffuses out of the sediments. Benthic denitrification can be comprised of essentially every denitrification process. While these different processes consume different forms of fixed nitrogen, they all produce $N_2$. Canonical denitrification, while less energetically favorable than oxic respiration, is one of the more energy efficient anoxic respiration pathways, and thus nitrate is typically the second electron acceptor depleted in a sediment column. The presence of the oxic-anoxic interface in sediments allows for coupled nitrification-denitrification to be a dominant form of denitrification in many benthic environments with oxic water columns, including the Bering Sea [*Granger et al.*, 2011]. This process results in very little drawdown of nitrate from the water column to support denitrification, but also reduces the amount of ammonium that diffuses into the water column after oxic respiration. While different denitrification processes consume different fixed nitrogen species, ammonium and nitrate are oxidized to nitrate in the oxic waters while transiting to the Canada Basin [*Nishino et al.*, 2005], thus preventing the need for a different N* definition. Additionally all denitrification processes have $N_2$ as an end product. Since much of

the fixed nitrogen consumed by benthic denitrification is sourced from organic matter degradation, phosphate is released in this process. Some of the phosphate is consumed by the burial processes discussed previously, and some of it reenters the water column. The different processes should have similar effects on both tracers in this region. These tracers have been used in conjunction previously to measure benthic denitrification in the Okhotsk Sea and been found to agree well [*Ito et al.*, 2014]. By observing these tracers in tandem, we can use their agreements and disconnects to elucidate where variations are caused by factors beyond denitrification.

This thesis walks through the nutrient, N*, and $N_2$/Ar results for each water mass in the Canada Basin, along with a brief history of those water masses in the results (Chapter 3). The discussion (Chapter 4) delves into the agreement and disagreement of $N_2$/Ar and N* in the Pacific water layer, and the ability of the tracers to quantify both biological and physical processes. We then introduce a model of deep benthic denitrification in the Canada Basin based on our paired tracers, and compare our rates with those in the literature from models and direct benthic measurements both locally and globally. We conclude (Chapter 5) with the relevance of these measurements, and the Canada Basin, to the global marine fixed nitrogen cycle.

# Chapter 2

# Methods

## 2.1 Field sampling

We collected CTD profiles and water samples on the Joint Ocean Ice Study (JOIS) in September and October 2015 aboard the *CCGS Louis S St-Laurent*. CTD profiles were taken using a rosette mounted Seabird 9/11 at fifty-four stations with seventy casts in the Canada Basin and on the Beaufort Shelf.

Nutrient samples were collected at all stations. At each station two sets of samples and duplicates were taken; one set was analyzed within 12 hours on-board, and one was frozen for analysis onshore. On-board samples were analyzed via an on-board three channel Seal Analytical nutrient Auto-analyzer following the methods laid out by the manufacturer. Standard calibration curves were run daily. If multiple stations were run within one day, a set of reference material was run between each station. Precision was determined to be 0.08 mmol $m^{-3}$ for $NO_3$ and 0.010 mmol $m^{-3}$ for $PO_4$.

We collected samples for $N_2$/Ar in two sets: one spatially distributed set of samples in the Pacific water layers; and one set of full depth profiles, based on samples taken in all water masses. All $N_2$/Ar samples were taken in duplicate. Pacific water

sampling focused on two isohalines: 32.6 and 32.9 (PSS-78), or in shallow casts the bottom depth. The full depth profile was constructed from three casts spread over two stations.

## 2.2 Sampling and measurement of $N_2$/Ar ratios

$N_2$/Ar ratios were measured following the method established in *Emerson et al.* [1999] with adaptations from *Manning et al.* [2010]; *Hamme and Emerson* [2013]. We sampled water for $N_2$/Ar analysis into evacuated 185mL glass flasks, which were poisoned with mercuric chloride ($HgCl_2$) and dried prior to evacuation. The flasks have Louwers-Hapert valves with two sealing O-rings [*Hamme and Emerson*, 2004]. A vacuum was maintained between the O-rings before sampling. The flasks were filled halfway with seawater from a Niskin bottle through tubing flushed with $CO_2$ to prevent atmospheric contamination. After sampling the necks and space between the O-rings were cleaned and filled with $CO_2$. Once back in the lab, a vacuum was pulled in the O-ring gap. We weighed the flasks, and then equilibrated the headspace in a rotating water bath for at least 8 hours. We then removed most of the water.

We purified the gas in the headspace with a liquid $N_2$ trap to remove water vapor and $CO_2$. The gas was then analyzed on a Finnigan MAT 253 stable isotope ratio mass spectrometer (IRMS) at the University of Victoria. The pooled standard deviation of the $N_2$/Ar duplicates from this cruise was $\pm 0.03\%$.

We express $N_2$/Ar ratios as supersaturation, the anomaly from equilibrium:

$$\Delta N_2/Ar = \frac{(N_2/Ar)_{meas}}{(N_2/Ar)_{equil}} - 1 \tag{2.1}$$

where $(N_2/Ar)_{meas}$ is the measured $N_2$/Ar ratio and $(N_2/Ar)_{equil}$ is the equilibrium ratio of $N_2$ and Ar given the potential temperature and salinity of the sample when

collected [*Hamme and Emerson*, 2004]. $\Delta N_2/Ar$ is represented as a percent.

To ensure sample quality, only samples where both duplicates were run and their standard deviations matched within ± 0.1%, slightly more than 3 times the pooled standard deviation (0.03%), are shown in the data reported in this paper.

Differences in the $O_2$ content on the sample and standard sides of the dual inlet mass spectrometer create differences in ionization efficiency, requiring correction [*Emerson et al.*, 1999]. We assume a linear relationship between the difference in the $O_2$ and the offset of the measured and actual ratios, although they have slightly non-linear correlations. Chemical slope corrections are determined from a series of standards with varying $O_2$ content and known $O_2/N_2/Ar$ ratios. The validity of these corrections is confirmed by running duplicate samples against standards with different $O_2$ content. If these duplicates had worse agreement than duplicates run against the same standard, this would indicate a problem. As seen in Table 2.1, there is no correlation between samples run against different standards and worse standard deviations. Additionally Figure 2.1 shows the $\Delta N_2/Ar$ profiles with and without chemical slope correction before quality control and indicates that while there are small corrections, the general trends stand regardless. The mean chemical slope correction caused a -0.0027% difference between the uncorrected and corrected $\Delta N_2/Ar$, and the largest correction created a difference of 0.0084% in the $\Delta N_2/Ar$ values.

**Table 2.1:** Standard deviation of duplicates separated by the standards each was run against. VONA1 has $O_2/N_2/Ar$ ratios similar to surface waters, while VONA2 has half the $O_2$ content of VONA1. If slope corrections were ineffective duplicate pairs run against different standards would have consistently worse standard deviations. Quality control removes any duplicates with standard deviations greater than 0.1

| Standard | Mean standard deviation (all samples) | Mean standard deviation (post quality control: standard deviation<0.1) |
|---|---|---|
| Both VONA1 | 0.026 (n=35) | 0.024 (n=34) |
| Both VONA2 | 0.070 (n=4) | 0.070 (n=4) |
| VONA1 and VONA2 | 0.045 (n=17) | 0.036 (n=16) |
| All | 0.035 (n=56) | 0.031 (n=54) |

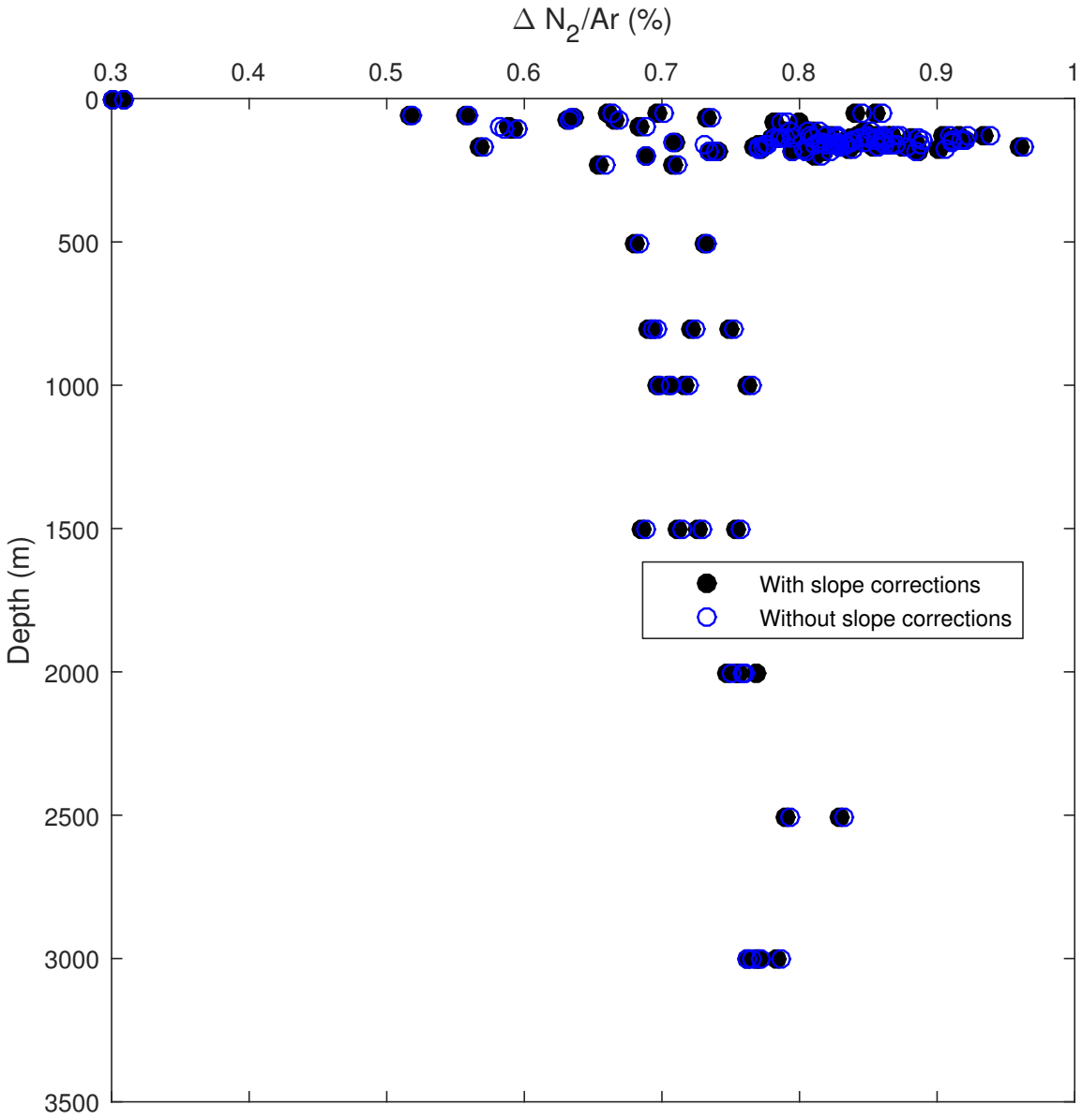


**Figure 2.1: $\Delta N_2/Ar$ profiles with and without chemical slope corrections and without any quality control**

# Chapter 3

# Results

## 3.1 Water masses in the Canada Basin

To understand the distributions of denitrification tracers in the Canada Basin, we need to consider the history of the water masses that layer over each other in this region. These water masses are primarily identified by their salinities and temperatures (Table 3.1), although, some have distinctive nutrient concentrations as well [*Cooper et al.*, 1997; *Codispoti et al.*, 2005, 2009; *Granger et al.*, 2011; *Brown et al.*, 2015]. The water masses observed in September and October 2015 (Figure 3.1) are similar to those previously described [*Codispoti et al.*, 2005]. All samples taken in the Canada Basin were targeted based on temperature and salinity rather than depth due to the variability in water mass depth throughout the Canada Basin. A brief introduction to each water mass is included below with the nutrient concentrations, N*, and $\Delta N_2/Ar$ results (Table 3.2).

**Table 3.1:** Definitions and depth ranges of Canada Basin water masses for this thesis. Definitions are predominantly salinity based, with temperature and salinity both defining the Atlantic Water (AW) and Deep Water (DW) and depth defining the Bottom Water (BW).

| Water Mass | Temperature Range °C | Salinity Range (PSS-78) | Depth Range (m) |
|---|---|---|---|
| Surface Water | not defined | <30 | 0-52 |
| Pacific Summer Water (PSW) | subsurface temperature maximum | 30-32.5 | 15-147 |
| Pacific Upper Halocline (PUHL) | temperature minimum | 32.5-33.5 | 6-218 |
| Lower Halocline (LHL) | not defined | 33.5-34.75 | 100-366 |
| Atlantic Water (AW) | >0 | >34.75 | 309-1005 |
| Deep Water (DW) | <0 | >34.75 | 1000-2700 |
| Bottom Water (BW) | <0 | >34.75 | 2700-bottom |

**Table 3.2:** Means, minimums and maximums of $NO_3$, $PO_4$, N* and $\Delta N_2/Ar$ by water mass

| Water Mass | | $NO_3$ (µmol $L^{-1}$) | $PO_4$ (µmol $L^{-1}$) | N* | $\Delta N_2/Ar$ (%) |
|---|---|---|---|---|---|
| Surface | Mean | 0.25 | 0.58 | -10.1 | 0.50 |
| | Minimum | 0.00 | 0.48 | -11.4 | 0.30 |
| | Maximum | 0.66 | 0.75 | -8.9 | 0.60 |
| PSW | Mean | 6.60 | 1.19 | -13.3 | 0.64 |
| | Minimum | 0.01 | 0.63 | -14.9 | 0.55 |
| | Maximum | 13.18 | 1.72 | -10.1 | 0.70 |
| PUHL | Mean | 14.82 | 1.80 | -13.9 | 0.83 |
| | Minimum | 11.16 | 1.46 | -16.2 | 0.72 |
| | Maximum | 16.56 | 1.99 | -8.8 | 0.93 |
| LHL | Mean | 13.39 | 1.14 | -4.9 | 0.72 |
| | Minimum | 11.48 | 0.83 | -11.6 | 0.72 |
| | Maximum | 15.53 | 1.67 | -0.8 | 0.72 |
| AW | Mean | 12.99 | 0.87 | -1.0 | 0.70 |
| | Minimum | 12.40 | 0.82 | -2.9 | 0.68 |
| | Maximum | 14.77 | 1.10 | -0.3 | 0.72 |
| DW | Mean | 13.97 | 0.96 | -1.3 | 0.75 |
| | Minimum | 12.45 | 0.86 | -2.2 | 0.69 |
| | Maximum | 15.10 | 1.06 | -0.8 | 0.83 |
| BW | Mean | 14.91 | 1.02 | -1.4 | 0.78 |
| | Minimum | 14.66 | 1.00 | -1.7 | 0.77 |
| | Maximum | 15.03 | 1.06 | -1.1 | 0.78 |

### 3.1.1 Surface Water

The uppermost waters of the Canada Basin referred to by some as the Polar Mixed Layer, are relatively fresh, the result of inputs from riverine and sea-ice melt inputs.

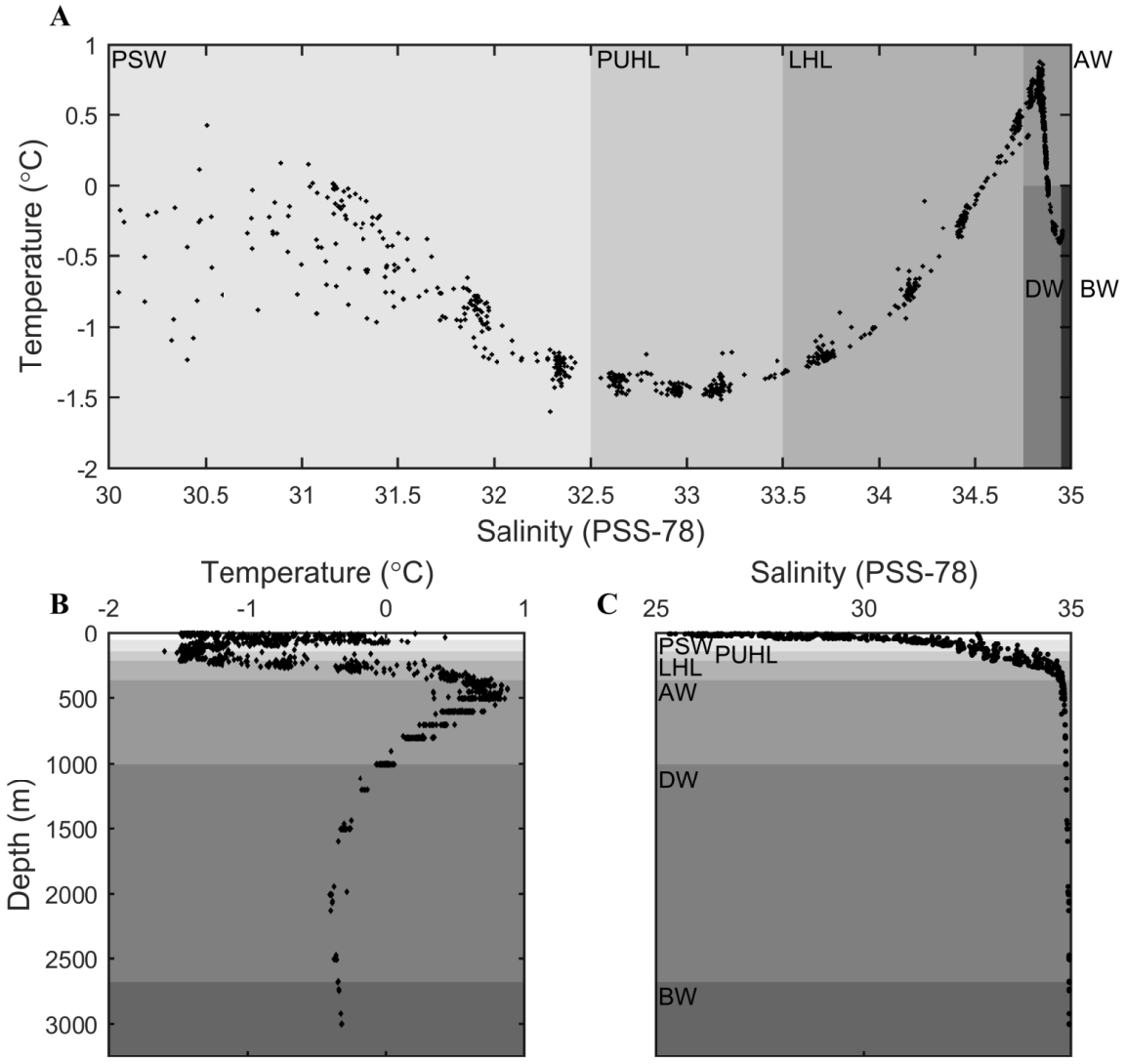


**Figure 3.1: Temperature and salinity from the Canada Basin. A** shows the T-S plot, with water masses indicated by the background shading. The same shading is used for plots **B** and **C** which show the temperature and salinity depth profiles respectively.

This layer is low in all nutrients (Figures 3.2 and 3.3), as it is the layer highest in biological productivity [*Macdonald et al.*, 2004]. The low nutrient renewal in this layer is due largely to the lack of vertical mixing caused by the intense salinity gradient [*Codispoti et al.*, 2005]; although, the seasonal effects of sea ice formation and melting result in mixing through destabilization of the stratification in winter [*Macdonald et al.*, 2004].

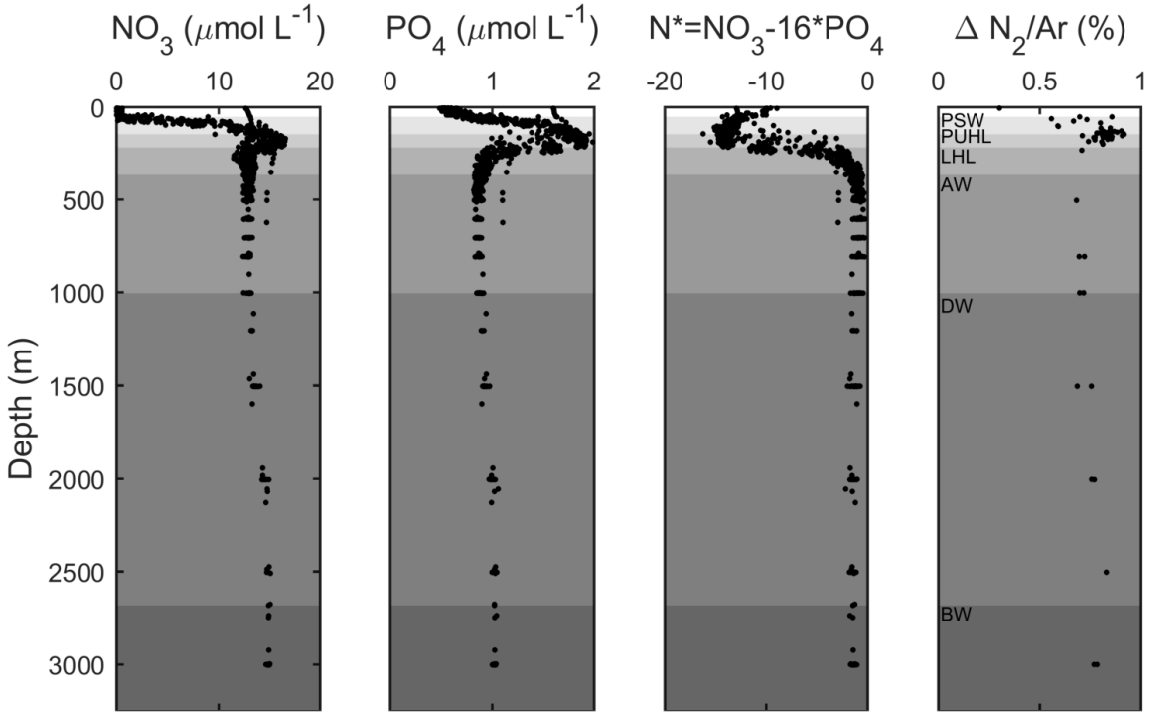


**Figure 3.2: $NO_3^-$, $PO_4^{3-}$, N* and $\Delta N_2/Ar$ profiles.**

While we observed both nutrients to have low values in the surface waters (0.0 to 0.66 µmol $L^{-1}$ for $NO_3$, and 0.48 to 0.75 µmol $L^{-1}$ for $PO_4$), the N* values are all strongly negative (-11.4 to -8.9). These results match with previous findings [*Codispoti et al.*, 2005] that inorganic nitrogen is often completely depleted in this layer without a corresponding exhaustion of phosphate. This indicates that the surface layer of the Canada Basin, the most productive layer, is severely nitrogen limited. A few $\Delta N_2/Ar$ samples were taken in this layer and show a broad range (0.30 to 0.60%). This range reflects measurements on mixed layer samples, which can exchange with the atmosphere and have low $\Delta N_2/Ar$ values, and deeper samples which no longer exchange with the atmosphere and match more closely with the underlying water masses.

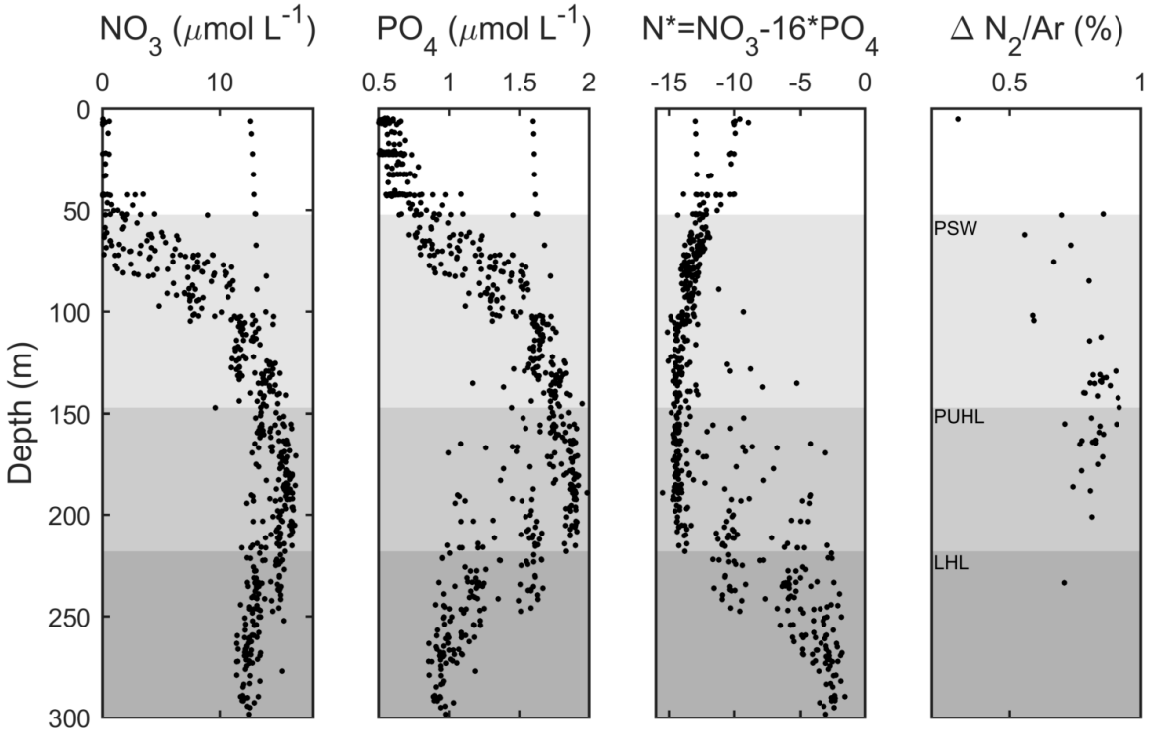


**Figure 3.3:** $NO_3^-$, $PO_4^{3-}$, N* and $\Delta N_2/Ar$ (%) upper 350m profiles.

### 3.1.2 Pacific Summer Water

Beneath the surface layer is the Pacific Summer Water Layer, defined by salinities between 30 and 33.5 (PSS-78) and the subsurface temperature maximum as seen in Figure 3.1 [*McLaughlin et al.*, 2004; *Nishino et al.*, 2008; *Timmermans et al.*, 2014]. This water was advected over the Bering and Chukchi shelves at the surface during the high productivity season and thus is lower in nutrients and higher in oxygen than water flowing over the shelves in winter [*McLaughlin et al.*, 2004; *Simpson et al.*, 2008].

A large range in both nutrients was observed (0.01-13.2 µmol $L^{-1}$ for $NO_3$, and 0.63 to 1.7 mmol $L^{-1}$ for $PO_4$) within this water mass, but more constrained ranges for N* (-14.9 to -10.1) and $\Delta N_2/Ar$ (0.55 to 0.70%) were observed. The variance in nutrient values is not surprising as the wide spread of temperatures and salinities (Figure 3.1)

implies that not all water within the PSW formed under identical circumstances.

However, the narrower ranges for both N* and $\Delta N_2$/Ar indicate that while the concentrations of nutrients vary, the nitrogen deficit does not. Here both the source and pathway of the water to the Canada Basin are important. The Pacific Ocean is a sink for fixed nitrogen due to the oxygen minimum zones of both the Eastern Tropical North and South Pacific and the lack of iron enrichment needed to stimulate nitrogen fixation. Additionally, water transiting from the Pacific to the Canada Basin moves over the Bering and Chukchi shelves, known hot spots for benthic denitrification with little seasonal variation [*Devol et al.*, 1997], which results in constant drawdown of nitrogen beyond the already low Pacific fixed nitrogen availability. The PSW carries the low nutrient concentrations associated with high levels of primary productivity and a signal of denitrification from the Pacific Ocean and its transit over the Bering and Chukchi shelves. We expect that our tracers act relatively conservatively in the Pacific water masses once these waters enter the Canada Basin due to a lack of contact with the atmosphere and minimal denitrification in the water column. This denitrification signal is weaker than that of the water mass directly below the PSW.

### 3.1.3 Pacific Upper Halocline Layer

The Pacific Upper Halocline Layer, also known as the Pacific Winter Water Layer, is defined by salinities between 32.5 and 33.5 (PSS-78) and the temperature minimum as seen in Figure 3.1 [*McLaughlin et al.*, 2004; *Nishino et al.*, 2008; *Brown et al.*, 2015]. It is also the layer with both the nutrient maximums (16 µmol $L^{-1}$ $NO_3$ and 2 µmol $L^{-1}$ $PO_4$) and the N* minimum (-15), properties previously mentioned in the literature [*McLaughlin et al.*, 2004; *Nishino et al.*, 2008; *Simpson et al.*, 2008; *Anderson et al.*, 2013; *Newton et al.*, 2013]. The nutrient and N* peaks, while broad, are concurrent as seen in Figure 3.4.

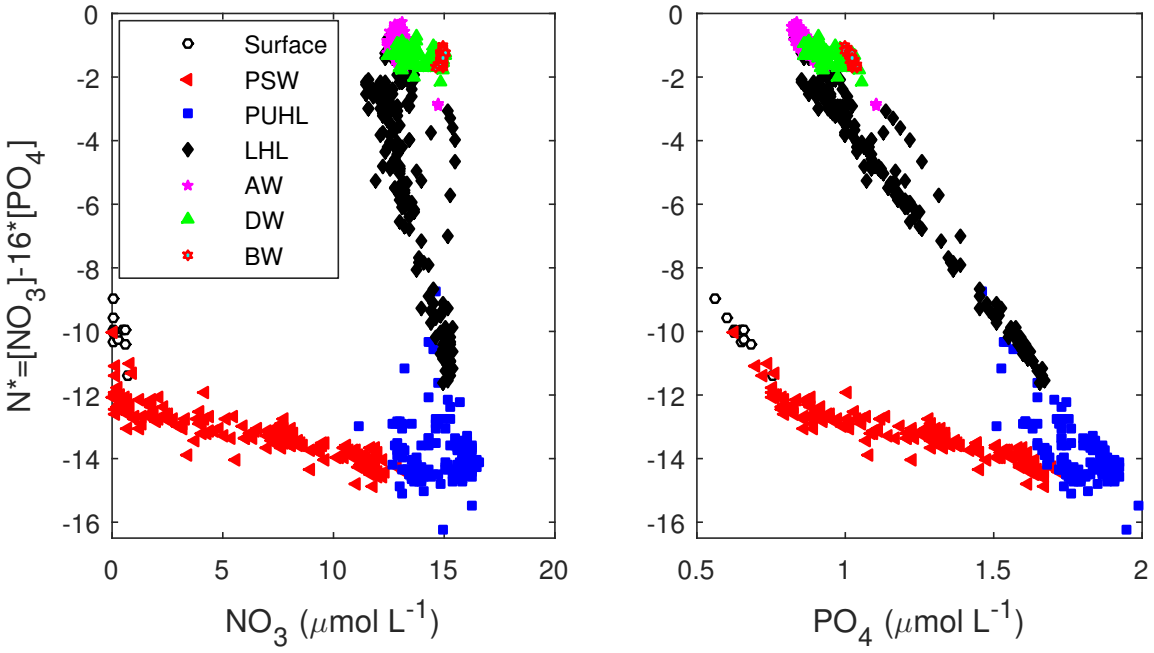


**Figure 3.4: N* versus $NO_3^-$ and $PO_4$.**

This concurrence is likely due to the formation of the water mass through advection along the bottom depths of the Chukchi shelf where it receives regenerated nutrients from the sediments and simultaneously gains a signal from benthic denitrification. One possible water mass formation history for the PUHL is through formation at polynyas via brine rejection causing the water to sink to the bottom where it gains its unique nutrient signature as it transits directly over the shelf sediments [*Pickart et al.*, 2005; *Itoh et al.*, 2012; *Souza et al.*, 2014]. However, *Pickart et al.* [2005] suggests that water formed via this method is actually too dense to remain in the upper halocline and is instead separate from Bering and Chukchi winter water. Nevertheless, the PUHL has nutrient concentrations which suggest that the water mass was bottom water for most of its transit across the shelves [*Codispoti et al.*, 2005].

While the nutrient and N* data collected match the literature, the $\Delta N_2/Ar$ results do not match expectations. Given the intense N* minimum, presumably caused by benthic denitrification on the Chukchi shelf, we expected to observe a strong $\Delta N_2/Ar$

signal in this water mass as well. The $\Delta N_2/Ar$ is elevated (0.83%), but this peak is much smaller than expected. We discuss this disconnect in Section 4.1.

### 3.1.4 Lower Halocline Layer

Under the PUHL is the Lower Halocline Layer (LHL), which has no strict definition but falls in the gap between the PUHL and Atlantic Water layer [*Simpson et al.*, 2008; *Newton et al.*, 2013]. Its nutrient and N* ranges also match this (Figure 3.5): $NO_3$ has a limited range (11.5 to 15.5 µmol $L^{-1}$) as the PUHL and AW layers have similar concentrations. $PO_4$ has a similar minimum (0.83 µmol $L^{-1}$) to the AW layer, but its maximum (1.7 µmol $L^{-1}$) is more representative of PUHL values. The differences in N* match with those in $PO_4$, with a very low minimum (-11.6) and a relatively high maximum (-0.8). Only one sample for $\Delta N_2/Ar$ was measured in this water mass. Its value (0.72%) falls between that of the PUHL and AW like the nutrients and N* values.

The LHL has the least well described source history. It largely forms on the Barents Sea shelf and undergoes modification by mixing north of the Barents Sea and by shelf inputs from the Eurasian and Chukchi shelves [*McLaughlin et al.*, 2004]. Both our measurements and previous measurements primarily show this layer as a transition zone between the Pacific and Atlantic water masses.

### 3.1.5 Atlantic Water

The LHL leads into the Atlantic Water (AW) layer, defined as having temperatures above 0 °C and salinities above 34.75 (PSS-78). The AW layer has the highest N* values (-2.9 to -0.3), due to its high $NO_3$ (12.4 to 14.8 µmol $L^{-1}$) and relatively low $PO_4$ (0.8 to 1.1 µmol $L^{-1}$) concentrations. Its $\Delta N_2/Ar$ range (0.68 to 0.72%) falls below that of the PUHL maximum but above that of the ventilated surface waters. This

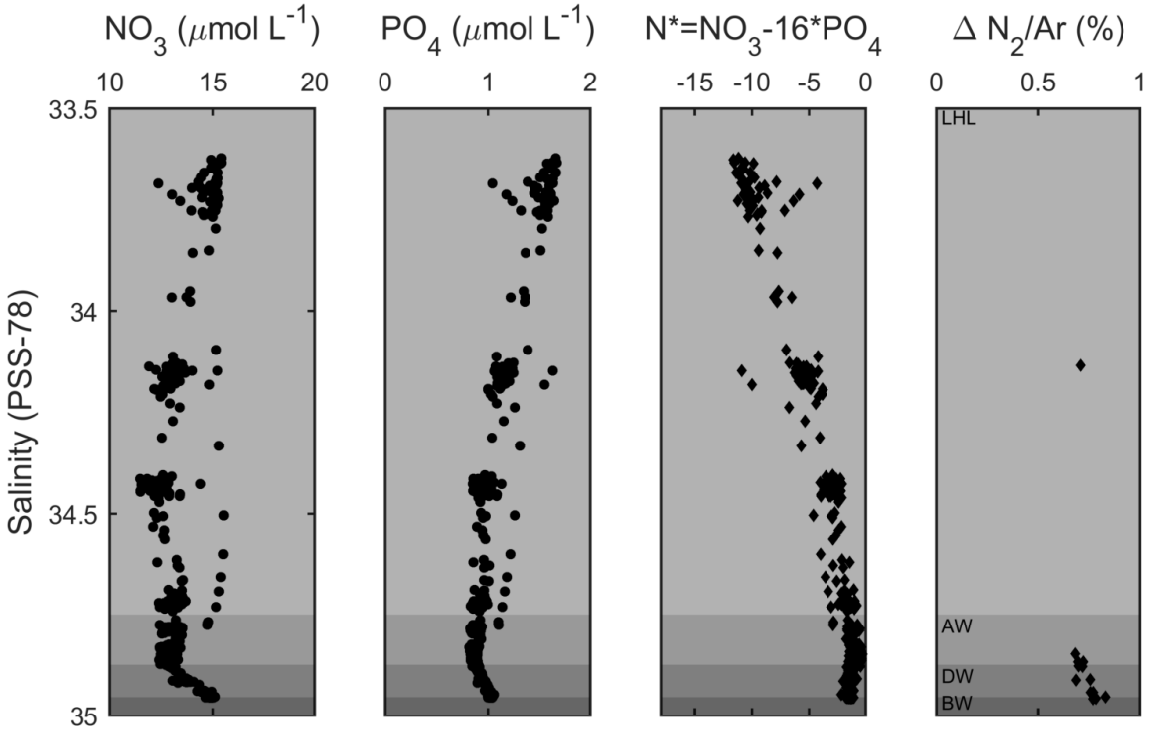


**Figure 3.5: $NO_3^-$, $PO_4^{3-}$, N*, and $\Delta N_2/Ar$ profiles versus salinity in the four deepest water masses.**

elevated $\Delta N_2/Ar$ signal is not unexpected as water masses that cannot exchange with the atmosphere preserve the signals of all physical and biological sources of dissolved gases. The AW is primarily formed from the Fram Strait Branch and the Barents Sea Branch of the inflow from the Atlantic Ocean [*McLaughlin et al.*, 2004; *Newton et al.*, 2013; *Zhong and Zhao*, 2014], thus matching water in the North Atlantic far more closely than the shallower Pacific waters of the Canada Basin. Our measurements of N* and nutrients in the AW layer match with previous measurements in the Canada Basin [*McLaughlin et al.*, 2004; *Codispoti et al.*, 2005, 2009] and with measurements in the literature for the North Atlantic [*Yamamoto-Kawai et al.*, 2006; *Deutsch and Weber*, 2012]. Additionally our measurements of $\Delta N_2/Ar$ match with measurements made in the Labrador Sea in the North Atlantic [*Hamme et al.*, 2017].

### 3.1.6 Canada Basin Deep and Bottom Waters

The deep waters of the Canada Basin are comprised of two layers with very similar temperatures and salinities. The upper layer extends from the bottom of the AW layer (1000m) to the sill depth (2400m) of the Alpha/Mendeleyev Ridges which separate the Marakov and Canada Basins [*Carmack et al.*, 2012; *Rudels*, 2015]. This water mass is often referred to in the literature as the Canadian Basin Deep Water. Below this layer, at a local temperature minimum, is a double diffusivity staircase approximately 300m thick which caps the bottom layer which is well mixed by geothermal heating, referred to as the Canada Basin Deep Water [*Carmack et al.*, 2012]. To avoid utilizing identical acronyms in this paper, these water masses will be referred to as the Deep Water (DW) and the Bottom Water (BW), respectively.

There are temperature and salinity differences between the DW and BW. Due to the geothermal heating, the BW has potential temperatures 0.01 °C higher than the temperature minimum which lies at the base of the DW [*Carmack et al.*, 2012]. Additionally, the BW has slightly higher salinities (0.005 PSS-78 higher) than the DW, thought to be caused by brine flowing off the shelves, although the frequency of these saline inputs is unknown [*Carmack et al.*, 2012]. For the purposes of this thesis, the distinction between these water masses is made solely on depth, and the double diffusive staircase is considered part of the DW.

Both deep water masses are relatively old; the DW is believed to have a residence time within the Arctic basins on the order of hundreds of years [*Codispoti et al.*, 2005]. The BW, however, is thought to have been isolated for approximately 450 to 500 years [*Macdonald and Carmack*, 1993; *Schlosser et al.*, 1997; *Timmermans et al.*, 2003; *Timmermans and Garrett*, 2006; *Carmack et al.*, 2012; *Rudels*, 2015]. This isolation is due largely to the double diffusive staircase separating the BW from the overlying water masses, and it is thought that the only inputs to the BW are saline

plumes mentioned above.

Both water masses have relatively high values for nutrients, N* and $\Delta N_2/Ar$ (Table 3.2). The DW has larger ranges for all parameters than the BW. The means for DW nutrients (14.0 µmol $L^{-1}$ $NO_3$ and 0.96 µmol $L^{-1}$ $PO_4$) and $\Delta N_2/Ar$ (0.75%) are higher than in the AW, and the average N* (-1.3) is lower than in the AW layer. In general, nutrients and $\Delta N_2/Ar$ increase with depth in the DW, while N* decreases with depth (Figure 3.6). The BW has very tight ranges for all parameters due to being well mixed by geothermal heating, with higher nutrients (14.9 µmol $L^{-1}$ $NO_3$ and 1.0 µmol $L^{-1}$ $PO_4$) and $\Delta N_2/Ar$ (0.78%) and lower N* (-1.4) than the DW. Unlike in the DW, in the BW there is little change with depth for nutrients, $\Delta N_2/Ar$, or N* (Figure 3.6).

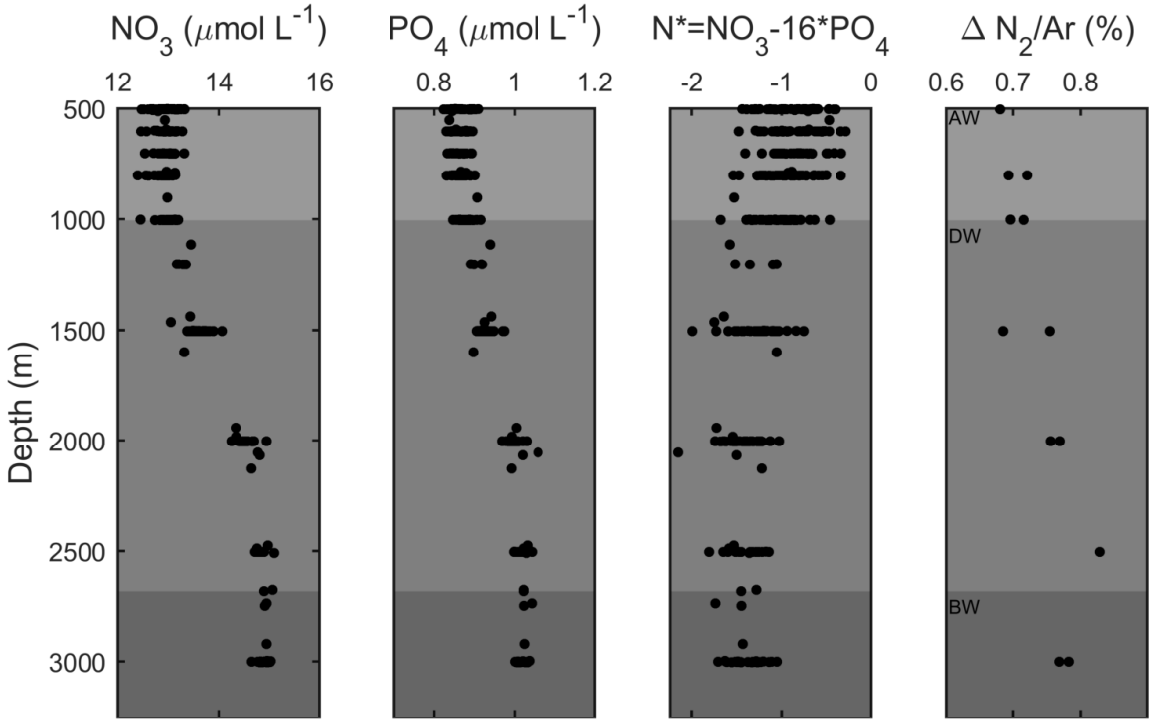


**Figure 3.6: $NO_3$, $PO_4$, N*, and $\Delta N_2/Ar$ profiles versus depth in the deep water masses.**

We hypothesize that benthic denitrification drives the pattern in the DW and

BW, and discuss this in Section 4.2.

# Chapter 4

# Discussion

## 4.1 Signals of denitrification in the Pacific Upper Halocline Layer of the Canada Basin

The $\Delta N_2$/Ar peak we observed in the Pacific Upper Halocline Layer (PUHL) was significantly smaller than we expected given the N* minimum in that layer. We expected that there would be a corresponding $\Delta N_2$/Ar peak in the same layer as the N* minimum due to the benthic denitrification on the Bering and Chukchi Shelves. Benthic denitrification should alter both tracers similarly and we do not expect there to be any processes altering these tracers once the Pacific water reaches the Canada Basin. While nitrogen fixation is occurring in the Canada Basin [*Blais et al.*, 2012], it shouldn't have any impact on the $\Delta N_2$/Ar [*Shigemitsu et al.*, 2016] and if it were affecting N* it would mean that the disconnect in denitrification signals we observe is underestimated. We approached the apparent disconnect between our tracers from several directions as laid out below.

Initial investigations into N* from previous years in the Canada Basin suggested a possible spatial pattern in N* related to time spent in the Beaufort Gyre, so we

looked for this pattern in the 2015 N* data and a similar pattern in $\Delta N_2/Ar$. To look for this correlation we plotted the spatial variability of $\Delta N_2/Ar$ and N* in the PUHL (Figure 4.1). There is no consistent pattern in the spatial variability of $\Delta N_2/Ar$ or N* in this layer, and a linear regression model had a $r^2$ of only 0.07. Additionally, neither tracer seems to vary with the anticyclonic (clockwise rotating) Beaufort Gyre. This indicates that the disconnect between our tracers develops before the water reaches the Canada Basin.

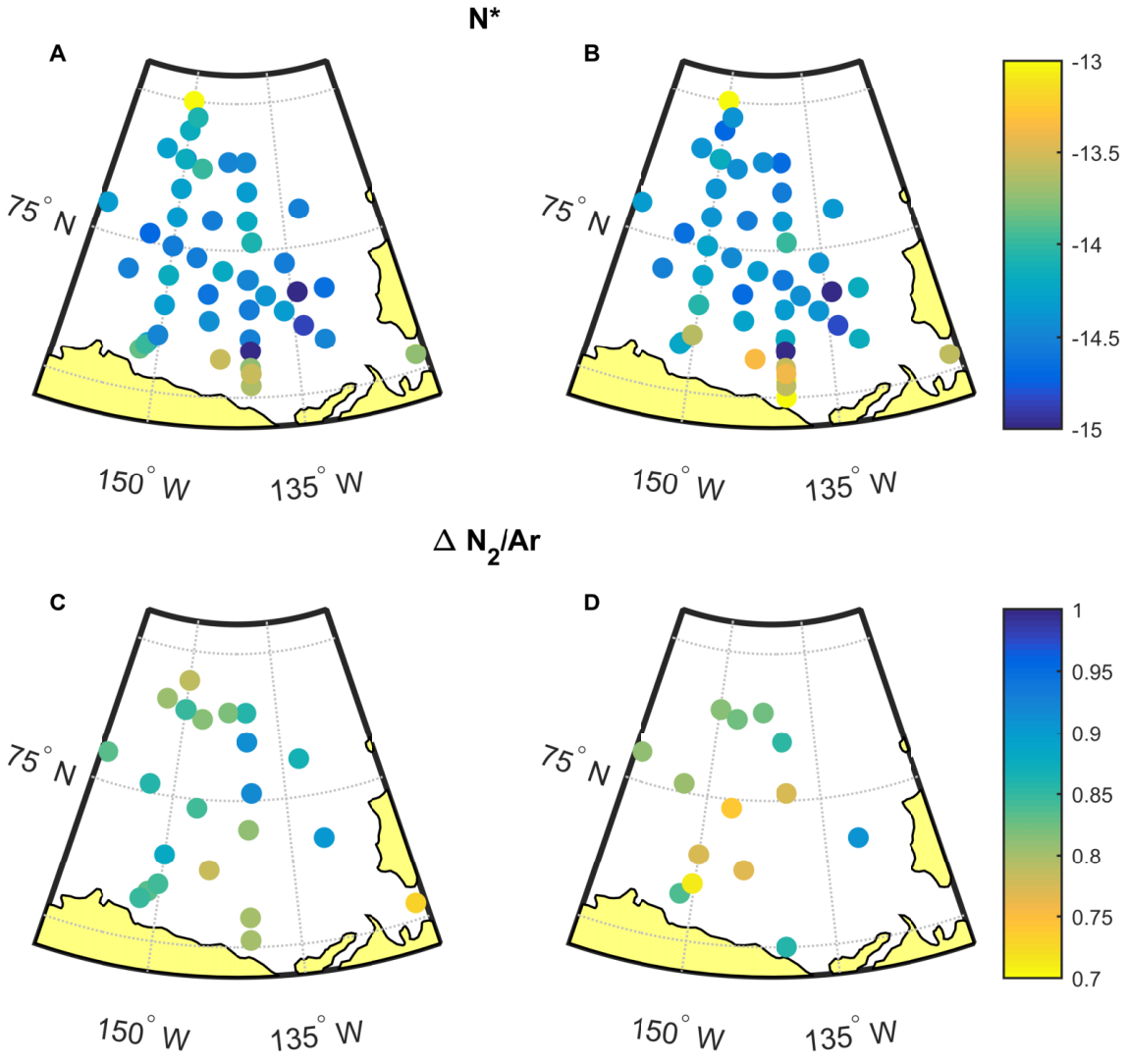


**Figure 4.1: Spatial distribution of N* (A and B) and $\Delta N_2/Ar$ (%) (C and D) on two isohalines:** 32.6 PSS-78 (**A** and **C**) and 32.9 PSS-78 (**B** and **D**).

To visualize and quantify this disconnect, we calculated the $\Delta N_2/Ar$ peak we expected in the PUHL based on denitrification estimated from the decrease in N* as the water moved from the North Pacific to the Canada Basin. We used two different estimates of the change in N* based on different initial conditions. The first is a realistic North Pacific N* of -6, based on data from LineP repeat transects to Station Papa in the NE Pacific [*Whitney and Freeland*, 1999] which has N* ranging from -6.5 to -5 in the upper 1000m; the second is an N* of 0, representing a scenario where $NO_3$ and $PO_4$ are colimiting, providing an extreme upper limit scenario. We calculated the decrease in N* between the assumed initial N* and the final N* measured in the PUHL of -13.9. Dividing by two and changing the sign, converts this decrease in N* to an expected increase in $N_2$ concentration which would be generated due to denitrification, $[N_2]_{add}$. We added this to the background $\Delta N_2/Ar$ in the PUHL, which we estimated to be the average of the bordering water masses (0.66%). Assuming that Ar in the water is similar to the expected equilibrium concentration, we can calculate the predicted $\Delta N_2/Ar$ as:

$$\Delta(N_2/Ar)_{pred} = \Delta(N_2/Ar)_{bkgd} + \frac{[N_2]_{add}}{[N_2]_{eq}} \tag{4.1}$$

where $[N_2]_{eq}$ is the $N_2$ concentration at equilibrium with the atmosphere for the temperature and salinity of the PUHL [*Hamme and Emerson*, 2004]. This calculation is similar in form to the $N_2$ excess calculation of *Manning et al.* [2010].

For a realistic N* change, the predicted $\Delta N_2/Ar$ is 1.25%. For the colimitation upper limit scenario, the predicted $\Delta N_2/Ar$ is 1.70%. The measured $\Delta N_2/Ar$ profile for the Canada Basin is plotted with these predicted values in Figure 4.2. The amount of denitrification suggested by N* would create a much larger peak in $\Delta N_2/Ar$ than we observed. The rest of this discussion uses the realistic N* change scenario.

To confirm this conclusion, we also calculated the starting N* given the final

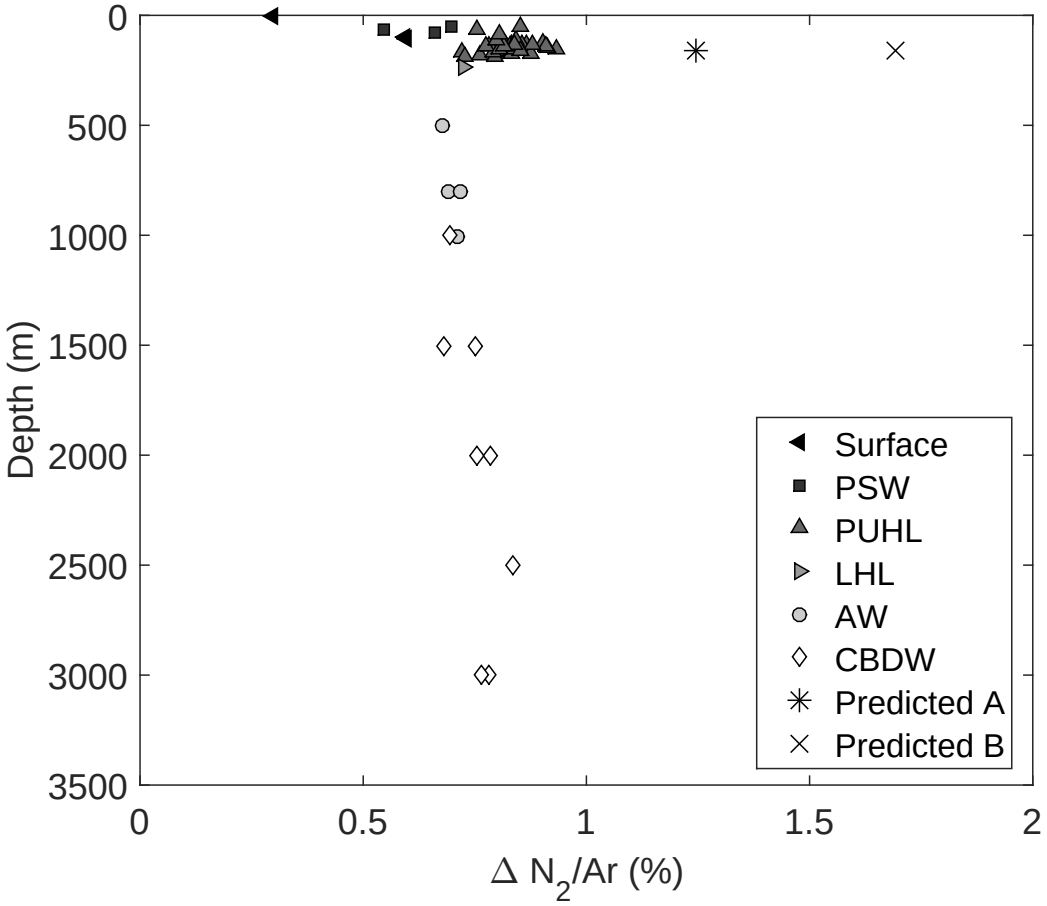


**Figure 4.2: Comparison of the $\Delta N_2/Ar$ profile with the predicted signal.** Two predicted $\Delta N_2/Ar$ values are shown: A is given an initial N* of -6 and B is given an initial N* of 0.

$\Delta N_2/Ar$ and N* values. We utilized the observed $\Delta N_2/Ar$ peak and the measured N* and obtained an initial N* of -11.7, much lower than the observed values in the North Pacific.

We suggest that the disconnect between the denitrification signal from N* and the signal from $\Delta N_2/Ar$ is caused by loss of $N_2$ to the atmosphere via ventilation on

the shallow Chukchi shelf. Most of the Chukchi shelf is approximately 50 m deep, and during ice-free periods intense winds can create deep enough mixing to mix the nutrient rich bottom water with the overlying surface waters [*Kawaguchi et al.*, 2015; *Nishino et al.*, 2015]. These mixing events, in addition to delivering nutrients to the surface waters, cause the loss of $N_2$ gas to the atmosphere thus dampening the $\Delta N_2$/Ar denitrification signal without altering the N* signal. This ventilation is likely highly seasonal, and dependent on both sea ice cover and wind speeds.

It is possible that this disconnect between the N* and $N_2$/Ar estimates of nitrogen loss could act as a downstream proxy for ventilation on the Chukchi shelf. While this study lacks measurements on the Chukchi shelf, we can utilize our endpoints and measurements of sedimentary denitrification from the literature to roughly estimate the ventilation occurring in the Chukchi Sea.

One approach to considering the ventilation occurring on the Chukchi shelf is to assume that denitrification occurs throughout the water's transit across the shelves but that thorough ventilation occurs for a certain portion of the water's transit such that the remaining $\Delta N_2$/Ar signal is from an unventilated end of the transit. This scenario suggests that the water column is ventilated for 72% of its journey across the Chukchi shelf.

A second approach is to assume that benthic denitrification and ventilation by gas exchange occur throughout the water's transit across the shelves at steady rates. In this case, the change in $N_2$ with time can be represented by:

$$h\frac{\delta N_2}{\delta t} = F_{[N_2]_{sedi}} - k([N_2]_{meas} - [N_2]_{bkgd}) \tag{4.2}$$

where $h$ is the water depth (m), $\frac{\delta N_2}{\delta t}$ is the change in $N_2$ concentration with time (mmol $m^{-3}$ $d^{-1}$), $F_{[N_2]_{sedi}}$ is the flux of $N_2$ from the sediment (mmol $m^{-2}$ $d^{-1}$), $k$ is the gas transfer velocity (m $d^{-1}$), $N_{2,meas}$ is the measured $N_2$ concentration (mmol $m^{-3}$)

from the PUHL, and $N_{2,bkgd}$ is the background $N_2$ concentration (mmol $m^{-3}$). The $N_{2,meas}$ and $N_{2,bkgd}$ terms are both determined from our $\Delta N_2/Ar$ measurements in the Canada Basin.

If we assume a steady state between the benthic flux of $N_2$ and the loss of $N_2$ due to gas exchange, the equation becomes:

$$([N_2]_{meas} - [N_2]_{bkgd}) = \frac{F_{[N_2]_{sedi}}}{k} \tag{4.3}$$

We can approach this equation from two directions: using estimates for the benthic $N_2$ fluxes, or using estimates for gas exchange in the Chukchi Sea.

*Chang and Devol* [2009] reports benthic $N_2$ fluxes to the water column of 1.6 mmol N $m^{-2}$ $d^{-1}$. Using this mean input along with the measured and background $N_2$ concentrations calculated from our data, we obtain a gas exchange coefficient of 0.73 m $d^{-1}$. Using the wind speed gas transfer velocity relationship reported by *Ho et al.* [2006], this equates to an average wind speed of 3.37 m $s^{-1}$. This wind speed is low for the Chukchi Sea, matching the lowest monthly average wind speed reported by *Stegall and Zhang* [2012].

We can take this same process in reverse and utilize the wind speeds reported by *Stegall and Zhang* [2012] to determine the benthic flux. The wind speeds range from a May minimum of 2-4 m $s^{-1}$ to an October maximum of 9 m $s^{-1}$. These wind speeds produce benthic fluxes of 0.56-2.3 mmol N $m^{-2}$ $d^{-1}$ and 11.4 mmol N $m^{-2}$ $d^{-1}$ respectively. The May wind speeds provide benthic fluxes within the range measured by *Devol et al.* [1997], and within a factor of two of the reported value from *Chang and Devol* [2009]. The October wind speeds give sediment inputs more than three times the highest sediment input (2.8 mmol N $m^{-2}$ $d^{-1}$) reported by *Devol et al.* [1997], thus warranting concern.

It should be noted that these calculations don't take into account the reduction

in gas transfer velocity caused by sea ice cover, which would reduce ventilation on the shelf, and thus lower the needed sedimentary inputs. The Chukchi Sea has highly seasonal sea ice cover, varying from 0% in summer months to essentially 100% [*Comiso and Parkinson*, 2008]. Given the variable nature of sea ice, we did not include fraction ice cover in Equation 4.3. However, it can be included as $k(1-f_{ice})$, showing that $k$ we solve for would be higher and more in-line with wind speed estimates if we accurately included the fractional sea ice amounts. Additionally these calculations ignore the effects of stratification on the water column. The Chukchi shelf has seasonally varying stratification with winter water dominating the water column in the winter, and being isolated to the bottom in summer [*Chu et al.*, 1999; *Weingartner et al.*, 2013]. This stratification may increase ventilation in the winter months, and decrease ventilation of the remaining winter water in the summer.

While the ranges of wind speeds and sediment inputs predicted by our calculation do not perfectly match the values reported elsewhere, they are within a factor of two to three of the values reported. Additionally, sea ice cover would decrease ventilation and make our predictions more accurate. Our measurements, and calculations based on them, provide strong support for the theory that ventilation on the Chukchi shelf causes a near equilibrium state for $N_2$ gas, with sedimentary inputs due to denitrification being matched by outgassing during the formation of the PUHL.

## 4.2 Remineralization and denitrification in the deep waters of the Canada Basin

The Deep Water of the Canada Basin (DW: 1000m to 2700m) has increases in nutrients and $\Delta N_2/Ar$ and a decrease in N* with increasing depth, whereas the Bottom Water (BW: 2700m to 3900m) has relatively constant profiles for nutrients, $\Delta N_2/Ar$

and N*. Given these observed shifts in $NO_3$, $PO_4$, N* and $\Delta N_2/Ar$ (Figure 3.6), our measurements suggest signals of benthic denitrification are being preserved in the deep waters of the Canada Basin. Our aim here is to quantify the rates of denitrification required for this signal to be apparent given the age of the water masses, and to put these signals in the context of global denitrification.

### 4.2.1 Methods for modeling nitrogen dynamics in the deep Canada Basin

To determine the rate of denitrification in the sediments of the Canada Basin and to explore the transport of denitrification signals through the water column, we built a 1D diffusion model based on Equation 4.4:

$$\frac{dC}{dt} = K_z \frac{d^2C}{dz^2} + C_{input} \tag{4.4}$$

where $C$ represents the concentration of one of our tracers, $t$ represents time, $K_z$ is the diffusivity, $z$ represents vertical distance, and $C_{input}$ is the change in concentration of the tracer due to denitrification (-N* or $+N_2$). The model runs over the Deep Water and Bottom Water from 1000m to the bottom (3900m), with 1m box heights. It moves forward in time over 500 years (the age of the Bottom Water mass) and ends in 2015 with time steps of half a year. We utilized a Crank-Nicholson discretization scheme as shown in Equation 4.5:

$$\frac{C_i^{t+1} - C_i^t}{\Delta t} = \frac{K_z}{2}\left(\frac{C_{i+1}^{t+1} + C_{i-1}^{t+1} - 2C_i^{t+1}}{(\Delta z)^2} + \frac{C_{i+1}^{t} + C_{i-1}^{t} - 2C_i^{t}}{(\Delta z)^2}\right) + C_{input} \tag{4.5}$$

this discretization is centered in space ($i$) and forward in time ($t$).

The model was tested with box heights ranging from 0.5-100m and time steps ranging from 0.25-2 years, yielding similar results. The model was initialized with uniform concentrations of each tracer tested, matching the concentration of the tracer at the bottom of the AW layer as measured in 2015. These initial conditions were chosen because while we lack understanding of the precise formation of these water masses, their temperature and salinity properties as well as their location in the water column make Atlantic waters the likely origin. Additionally, the AW is the water mass with the most similar conditions to those found in the DW and BW.

The shallow boundary condition is $C^{t+1}_{shallow} = C^{t_0}_{shallow}$ to fix the shallow concentration at the AW value. This boundary condition allows for the signals to diffuse across the boundary and be lost. Comparison of the change in the inventory of the water column with the total concentration added shows that 44% of the inputs diffuse are lost over the course of the model. The deep boundary condition is $C^{t+1}_{bottom} = C^{t+1}_{bottom-1}$ so that it accumulates the benthic inputs with no flux across the bottom boundary.

Denitrification rates were included in the model as a loss of fixed nitrogen in the form of a decrease in N* or an increase in $N_2$. Ranges for the total inputs to the water column were based initially on data from other deep basins (Table 4.2) and varied to match the observed tracer concentrations. The initial iteration of the model had all the inputs in the deepest box. However, this produced exponential profiles with upward concavity, very different from the observed results. To remedy this disagreement, we distributed the inputs across the boxes of our model based on the fractional area each depth comprises in the deep Canada Basin from the ETOPO1 dataset as seen in Figure 4.3. The majority of the deep Canada Basin has depths greater than 3000m, which causes most of the benthic inputs to occur in the BW. Given that horizontal mixing would need to be higher to support homogeneity higher in the water column, the low percentage of benthic inputs occurring there improves

our model's ability to accurately predict denitrification rates.

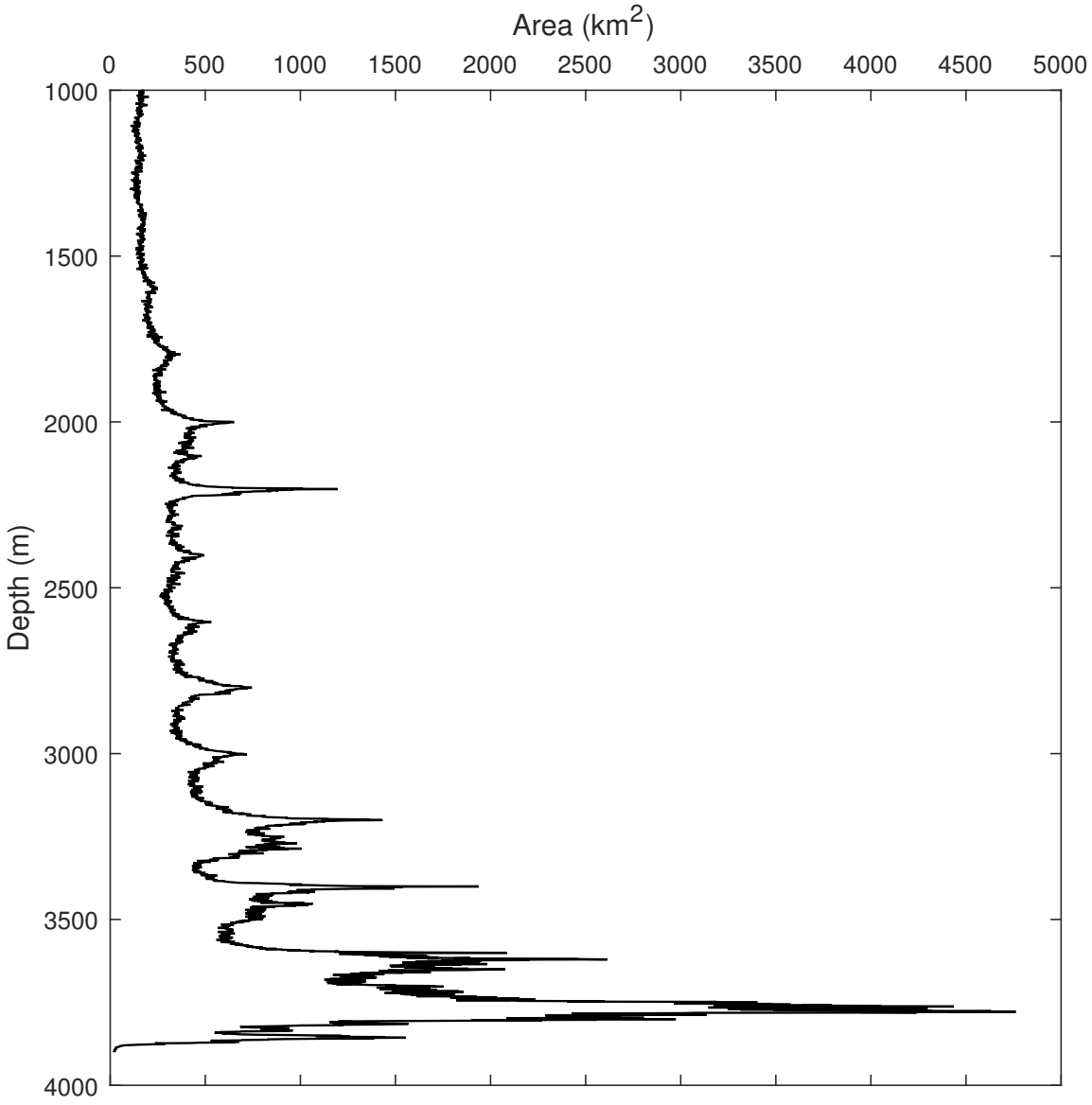


**Figure 4.3:** Area based distribution of depths in the deep Canada Basin

We utilized the diffusion rate for the DW reported by *Macdonald and Carmack* [1993] of $3.9 * 10^{-5}$m$^2$ s$^{-1}$. This diffusion rate was determined from a similar 1D diffusion model based on $^{14}$C data [*Macdonald and Carmack*, 1991, 1993]. The diffusion rate for the geothermally mixed BW is $8 * 10^{-4}$m$^2$ s$^{-1}$, representing the fifteen day mixing time determined from a rotating convective vertical velocity scale reported by

*Carmack et al.* [2012].

There are several key features of the deep Canada Basin we could not account for in this model but which are worth identifying. The winding flow paths of these deeper waters, despite their similar sources in the various Arctic basins, cause time lags and interactions with boundary currents result in different properties in the different Arctic basins [*Rudels*, 2009]. The Canada Basin acts essentially as the last stop before the Atlantic origin and deeper waters flow back towards the Atlantic Ocean. Advection of water from the Makarov Basin into the DW causes the temperature minimum layer at the double diffusive staircase. However, we did not include this because we not only lack constraints on the amount of advection occurring, but also what the signal of our tracers is in the incoming water from the Makarov. The second is the role of horizontal mixing. While the bottom waters do directly receive benthic inputs, higher in the water column much of the water is not in contact with the benthos. The model assumes that the layers are horizontally homogenous. Essentially assuming that there is fast horizontal mixing which is not true, but given the time scales isn't an inherently invalid assumption. A recent modeling study investigated the role of mesoscale eddies in the Beaufort Gyre on horizontal diffusivity in the halocline layers which may able to inform horizontal diffusivity in deeper waters and provide an estimate of horizontal mixing time scales [*Manucharyan et al.*, 2016]. We additionally did not include the double diffusive staircase as a separate layer due to a lack of constraints on non-thermal diffusivities in this layer. It is important to note that we do not expect that the double diffusive staircase would significantly affect $\Delta N_2/Ar$ values.

The aim of this model is not to find a steady state condition for the deeper waters of the Canada Basin, but rather to attempt to use modeling to determine the rates of denitrification required to accumulate the signals we observe given the age of the

Bottom Water. To determine if the model was approaching steady state, we ran it for 2000 years and plotted the profile every 500 years in Figure 4.4. As can be seen, at 500 years the model is not at steady state.

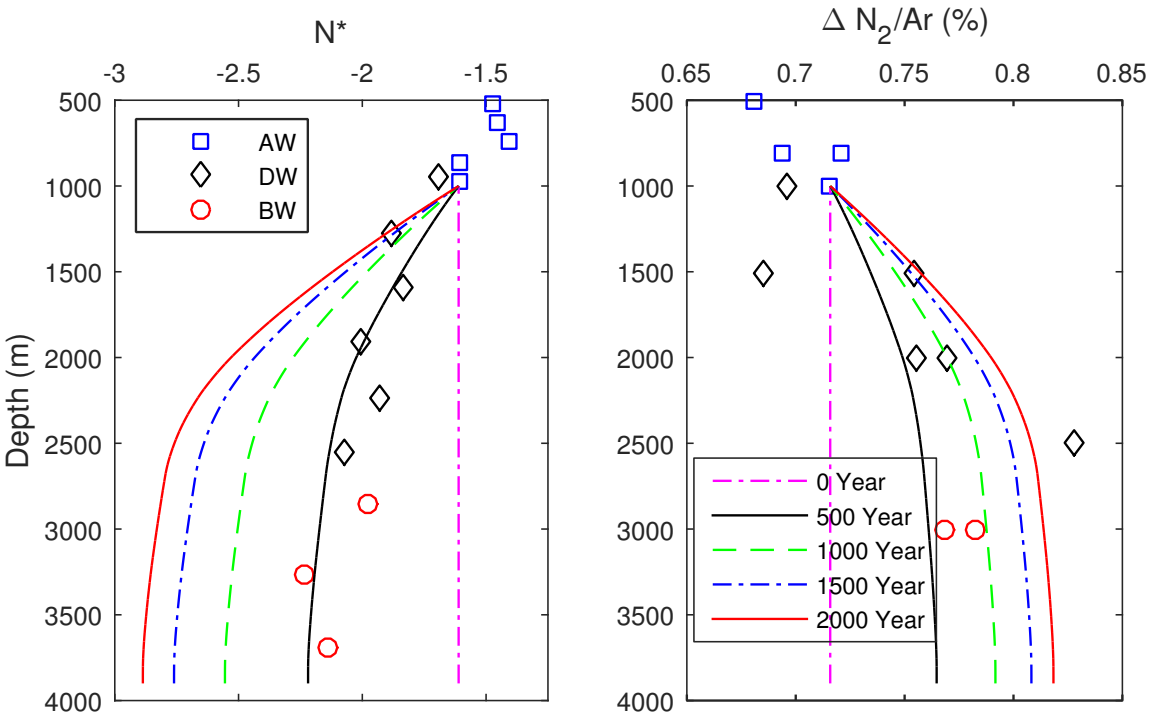


**Figure 4.4:** Profiles of N* and $\Delta N_2/Ar$ from year 0, 500, 1000, 1500 and 2000 of the model. Measured values for both tracers are shown in the symbols. The input for this model was 0.0125 mmol N $m^{-2}$ $d^{-1}$.

### 4.2.2 Modeled deep nitrogen dynamics in the Canada Basin

A root-mean-square error analysis (Table 4.1) indicates that the best fits from our model are 0.0109 mmol N $m^{-2}$ $d^{-1}$ for the N* data, and 0.0191 mmol N $m^{-2}$ $d^{-1}$ for the $\Delta N_2/Ar$ data. Benthic denitrification fluxes determined from our model (Figure 4.5) fall on the low end of reported denitrification rates from other deep basins (Table 4.2). Reported rates of denitrification from direct measurements in the Atlantic range from 0.024 to 0.06 mmol N $m^{-2}$ $d^{-1}$ [*Martin and Sayles*, 2004; *Trimmer and Nicholls*, 2009] and 0.05 to 0.110 mmol N $m^{-2}$ $d^{-1}$ in the Northeast Pacific [*Engstrom et al.*, 2009].

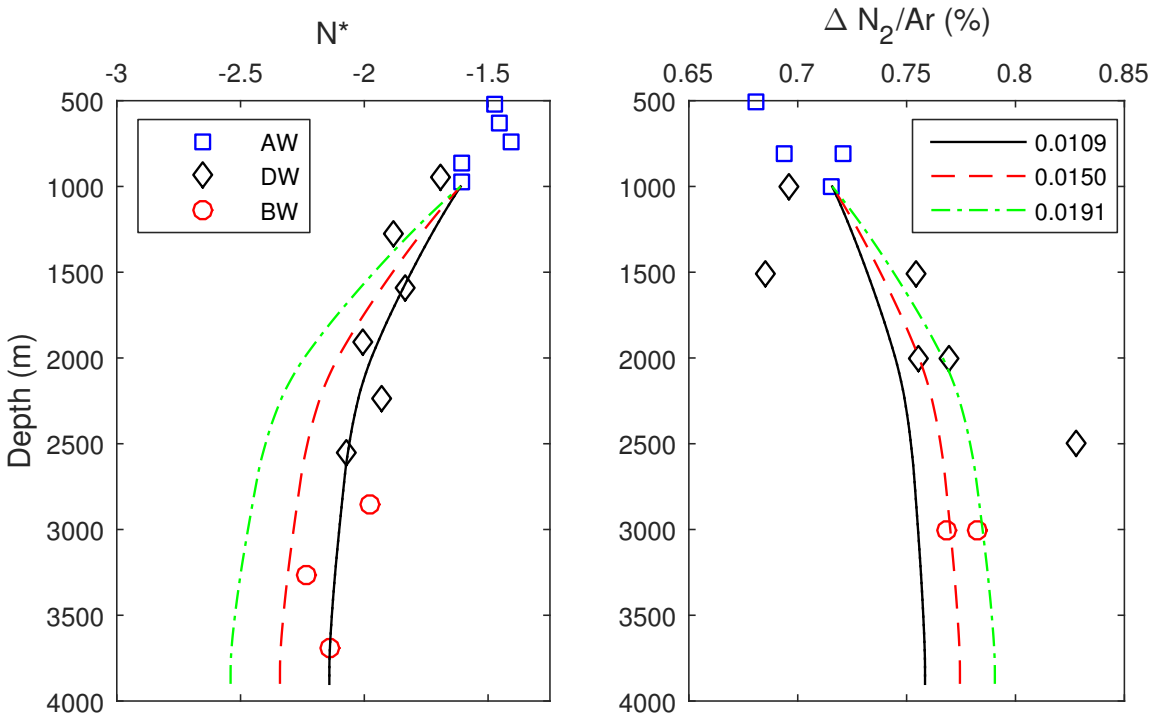


**Figure 4.5: Measured and modeled profiles of N* and $\Delta N_2/Ar$ in the DW and BW.** Measured values are symbols and modeled values are lines, with the inputs in mmol N $m^{-2}$ $d^{-1}$.

*Chang and Devol* [2009] made limited measurements off the Chukchi shelf into deeper waters (1000-4000m); the estimates they obtained had a wide range (0.00-0.118 mmol N $m^{-2}$ $d^{-1}$) but again match our estimates. A model of benthic denitrification rates by *Middelburg et al.* [1996] estimated deep benthic denitrification rates ranging from 0.0114 mmol N $m^{-2}$ $d^{-1}$ at 4000m to 0.6564 mmol N $m^{-2}$ $d^{-1}$ at 1000m. On a basin wide scale, our model predicts that sediments deeper than 1000m in the Canada Basin remove 0.083-0.145 Tg N $y^{-1}$, or less than 0.1% of annual global denitrification.

**Table 4.1:** Root-mean-square (RMS) errors of modeled denitrification inputs

| Modeled denitrification rate (mmol N $m^{-2}$ $d^{-1}$) | N* RMS error | $\Delta N_2/Ar$ RMS error |
|---|---|---|
| 0.0109 | 0.0903 | 0.0362 |
| 0.0150 | 0.1777 | 0.0310 |
| 0.0191 | 0.3190 | 0.0291 |

*Middelburg et al.* [1996] also points out that benthic denitrification rates are primarily controlled by the total remineralization rate, carbon flux, and bottom water $O_2$ and $NO_3$ conditions. Thus our denitrification rates agree with the conclusion of *Macdonald and Carmack* [1993]: Remineralization rates, determined from oxygen utilization rates, in the deep Canada Basin are approximately half those in the deep Atlantic. Given the low remineralization and denitrification rates, as well as the age of the water mass and its high oxygen content, it is likely that the organic matter entering the Bottom Water is relatively recalcitrant, that the total flux is small, and that denitrification makes up a small proportion of the overall remineralization.

**Table 4.2:** Denitrification Rates in Deep Sediments

| Region | Denitrification rate (mmol N $m^{-2}$ $d^{-1}$) | Depth (m) | Source |
|---|---|---|---|
| North Atlantic | 0.024-0.06 | 2000 | *Trimmer and Nicholls* [2009] |
| Northwest Atlantic | 0.0329 | 2510 | *Martin and Sayles* [2004] |
| Cascadia Basin | 0.05-0.110 | 2800-3100 | *Engstrom et al.* [2009] |
| Global (modeled) | 0.0114-0.6564 | 1000-4000 | *Middelburg et al.* [1996] |
| Off-shelf Chukchi Sea | 0.00-0.118 | 3000-3210 | *Chang and Devol* [2009] |
| Canada Basin | 0.01-0.04 | 1000-4000 | this study |

Of note in the model results is the disconnect between N* and $\Delta N_2/Ar$ changes which are not occurring at matching rates (Figure 4.5). The change in N* from the bottom of the AW to the BW is -0.50, and the change in $\Delta N_2/Ar$ from the bottom of the AW to the BW is 0.06%. From the observed change in $\Delta N_2/Ar$ we would expect an N* of -0.77, 50% larger than observed. As a result, we have two sets of available N loss rates from the model, one matching each tracer's observed profile. Possible reasons for the difference in the changes of N* and $\Delta N_2/Ar$ include: increased $N_2$ concentrations in the BW due to physical processes, difficulty accurately quantifying such low changes in $\Delta N_2/Ar$, and high N:P ratios in sinking organic matter.

Several physical processes differently affect $N_2$ and Ar dissolution in water. The most important of these is bubble injection, which increases $\Delta N_2/Ar$. Bubble injection and denitrification are the two processes most likely to cause changes in $\Delta N_2/Ar$

[*Hamme and Emerson*, 2013]. In addition to waves driving bubbles into the surface waters during convection events, glacial meltwater can also add air to water masses and elevate $\Delta N_2/Ar$. The only other process which increases $\Delta N_2/Ar$ is rapid cooling, but this process has minimal effects on the ratio [*Hamme and Emerson*, 2013]. It is possible that the initial formation event of the BW resulted in higher $\Delta N_2/Ar$ through physical processes occurring during the formation event such as high bubble injection.

It is also notable that the changes in $\Delta N_2/Ar$ are at the limit of detection. The pooled standard deviation of our samples in the Canada Basin is 0.03%, giving us a limit of detection of 0.09%, slightly larger than the observed change (0.060%). Given the corroboration of N* data, we consider these measurements to be of use; however, future sampling should focus on elucidating this signal and verifying the disconnect between N* and $\Delta N_2/Ar$.

N* relies on organic matter having the canonical Redfield N:P ratio. If organic matter being exported in the Canada Basin has a higher N:P ratio, when remineralized, even in the absence of denitrification, N* will increase as more nitrate is being released than expected given the phosphate released. Ratios ranging from 5 to 33.5 have been observed in global oceans, and tend to vary off the canonical value when one nutrient is depleted and the other is taken up as luxury uptake [*Deutsch and Weber*, 2012]. Measurements on the Chukchi Shelf provide support for non-Redfield N:P utilization ratios, but generally show lower ratios than the canonical value [*Mills et al.*, 2015; *Piper et al.*, 2016], which cannot explain our disconnect. More measurements of $\Delta N_2/Ar$ and possibly direct measurements of benthic fluxes in the deep Canada Basin are necessary to understand this tracer disconnect.

Our data and model independently agree with the existing literature with regards to the general rates of denitrification in the deep Canada Basin relative to rates in

other deep ocean basins. While the deep Canada Basin itself has a small role in the global denitrification rate, there remains a need to collect more data in the deep Canada Basin and other deep basins to understand their collective role in the global nitrogen cycle. These measurements should include direct measurements of sediment fluxes, as deep ocean sediments cover a far larger area than shallow shelves.

# Chapter 5

# Conclusion

This study presents some of the first measurements of $\Delta N_2/Ar$ in the Arctic Ocean and provides an opportunity to consider the biological and physical processes essential to the transformation of water transiting from the Pacific to the Atlantic by way of the Arctic. In the PUHL, the $\Delta N_2/Ar$ denitrification signal appears to be partially lost, preventing our ability to estimate net denitrification from the Chukchi from this tracer. However, this disconnect can act as a proxy for ventilation rates on the Chukchi shelf during winter months. While $\Delta N_2/Ar$ is a useful tracer of denitrification in deeper waters, denitrification occurring in partially ventilated shelf waters is underestimated in $\Delta N_2/Ar$ measurements.

We made limited measurements of $\Delta N_2/Ar$ in the deep waters, but a 1D diffusion model of denitrification inputs supports previous estimates of denitrification rates in the Canada Basin compared with global rates. Despite low temperatures and total remineralization rates, the deep Canada Basin, covering only 0.4% of the global ocean area, contributes approximately 0.1% of the global denitrification. While the deep Canada Basin alone does not contribute significantly to the global denitrification rate, it does highlight the importance of taking into account areas with low rates, as over

80% of ocean depths are greater than 3000m. Our measurements are a reminder of the importance of incredibly slow rates occurring over large areas.

Additional measurements are needed along other portions of the pathway of Arctic water to aid in distinguishing between biological and physical processes, such as ventilation and sea ice formation and melting, affecting $\Delta N_2/Ar$. The Arctic Ocean is a well known hot spot of denitrification on the shelves [*Devol et al.*, 1997; *Chang and Devol*, 2009; *Souza et al.*, 2014]. A more complete understanding of rates both and off the shelves in the Arctic will help to solidify our understanding of the global marine nitrogen budget. With a more extensive dataset, $\Delta N_2/Ar$ may help to elucidate interactions between the myriad physical processes altering Arctic water, and provide insight into the importance of denitrification in largely inaccessible sediments to the global budget.

# Appendix A

# GEOTRACES

The final passage of water from the Pacific into the Atlantic is largely through the Canadian Arctic Archipelago (CAA) and Baffin Bay (BB). From BB, the water exits the Arctic and re-enters the global thermohaline circulation in the Labrador Sea (LS) (Figure A.1). Our samples in this region are primarily from the 2015 Canadian Arctic GEOTRACES program, with supplemental data from repeat cruises in the LS. The stations used in this data set are shown in Figure A.2.

Casts on the Canadian Arctic GEOTRACES 2015 program were conducted with a Niskin bottle rosette and attached Seabird SBE 9 CTD. Nutrient samples were run by the lab of Jean-Éric Tremblay. $\Delta N_2/Ar$ samples were collected and analyzed in the same manner as the Canada Basin samples.

The goal of this appendix is to lay out the work that has already been conducted on this dataset, so as to relieve future efforts from having to repeat any work. The primary issue at hand with this data is a lack of agreement between $\Delta N_2/Ar$ and N* which has yet to be reconciled despite our efforts. Outlined below are our results, and the investigations conducted into the disconnect to date.

Select temperature and salinity data from the 2015 Canadian GEOTRACES pro-

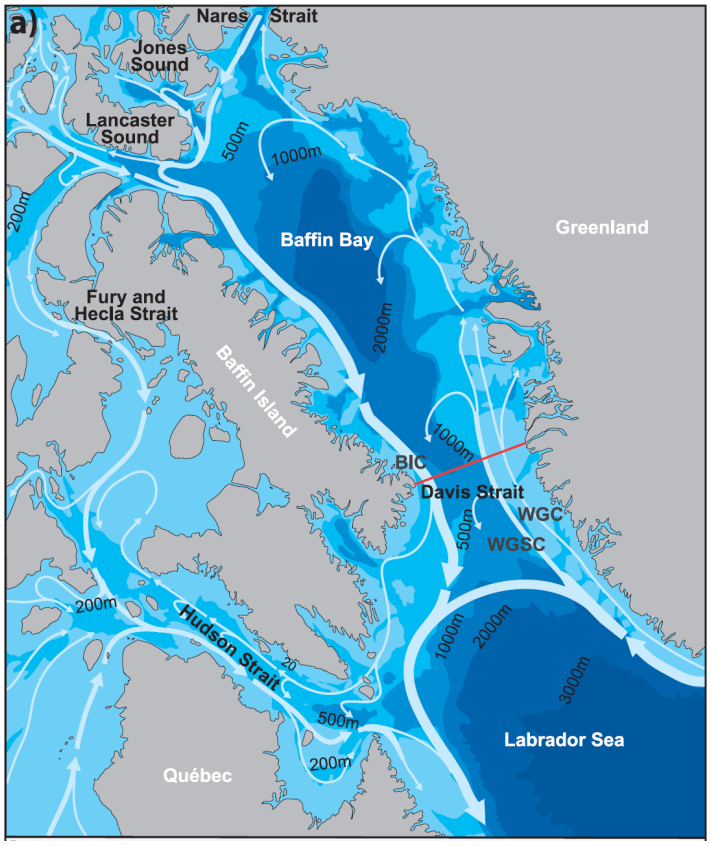


**Figure A.1:** Circulation in and around Baffin Bay, from [*Curry et al.*, 2011]

gram are shown in Figure A.3. Water in this region is from two sources: the Labrador Sea and flow through from the Arctic via the CAA. In Baffin Bay it circulates in a counter-clockwise direction, exiting through the western side of Davis Strait (Figure A.1). The BB has three main water masses: the Polar Water, the West Greenland Intermediate Water, and the BB Deep and Bottom Waters. The Polar Water is cold (<0°C to the temperature minimum) and fresh (33.7). It forms from a mixing between the upper layer of water entering through Davis Strait which cools as it circulates around BB, and the inflow of upper Arctic water through Lancaster, Jones and Smith Sounds. The West Greenland Intermediate Water is warm (>0°C) and salty (>34) and dominated by inflow through the eastern Davis Strait and occupies depths of 300 to 800m. The temperature maximum which occurs in this layer decreases as

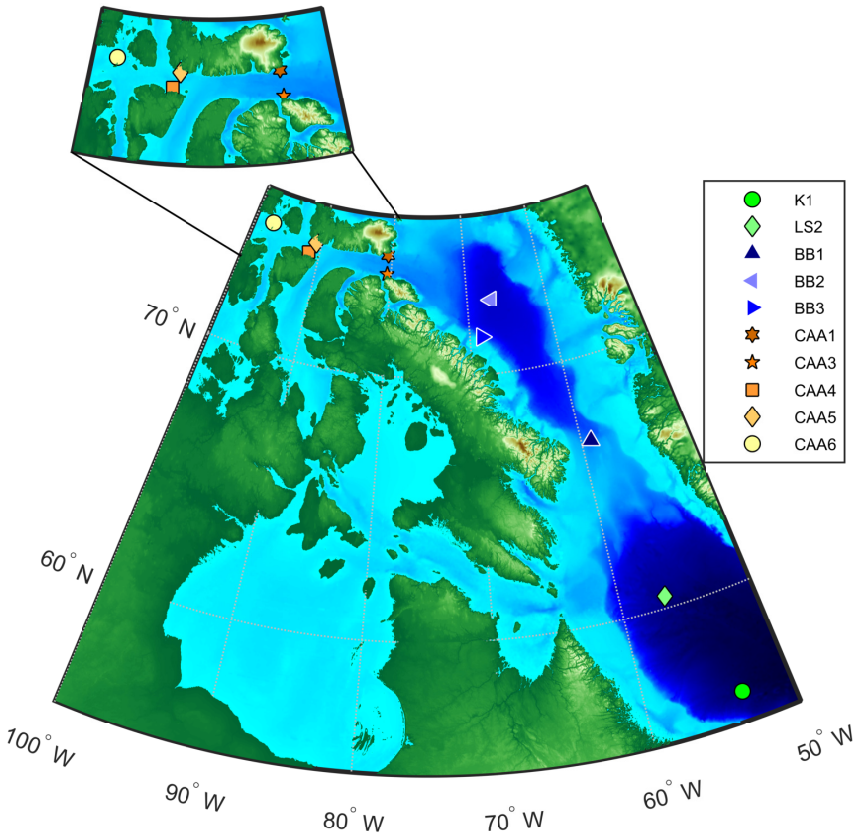


**Figure A.2: Station map for $\Delta N_2/Ar$ samples from Canadian Arctic GEOTRACES.**

the water circulates around BB. The BB Deep (1200-1800m) and Bottom (>1800m) waters have fairly constant salinity (<34.5) and slowly decreasing temperature (to a bottom temperature of -0.5°C).

N* for all stations has a minimum near 100m, and then increases into the subsurface waters (Figure A.4). In BB N* decreases again in waters deeper than 400m. The Labrador Sea N* has a small minimum and then very vertical, near 0 profile at all depths greater than 200m. CAA profiles are more variable, with deep waters matching the BB profiles.

Given what we observe in N*, we expected to see $\Delta N_2/Ar$ profiles in BB and the CAA which were low around 400m and increased in the deep water. Instead, $\Delta N_2/Ar$ increases with depth to 400-600m and then has little increase in the deep

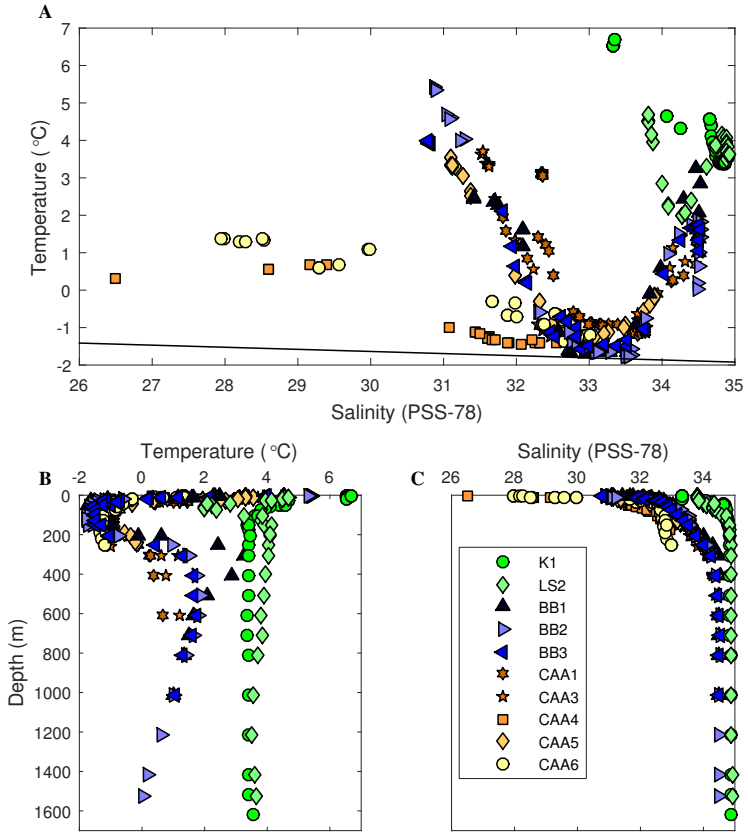


**Figure A.3:** **a** Temperature versus salinity, **b** temperature and **c** salinity versus depth

water (Figure A.5). Labrador Sea $\Delta N_2/Ar$ values from this cruise match well with previous data collected in the Labrador Sea by our lab. Generally, Labrador Sea profiles are low in the surface, and increase to approximately 0.8% in the subsurface with near constant values for the rest of the water column due to convection. BB and CAA profiles are initially low, and increase past the Labrador Sea profile by 200m. One Baffin Bay station and one CAA station continue to increase to their maximum depth, with $\Delta N_2/Ar$ values greater than 1.5%. These values for $\Delta N_2/Ar$ are among the highest seen in the world's oceans, even in oxygen minimum zones [*Chang et al.*, 2010, 2012; *Hamme and Emerson*, 2013].

To illustrate the disconnect between the N* and $\Delta N_2/Ar$ profiles, we calculated the N* profile we would have observed if the denitrification indicated by $\Delta N_2/Ar$

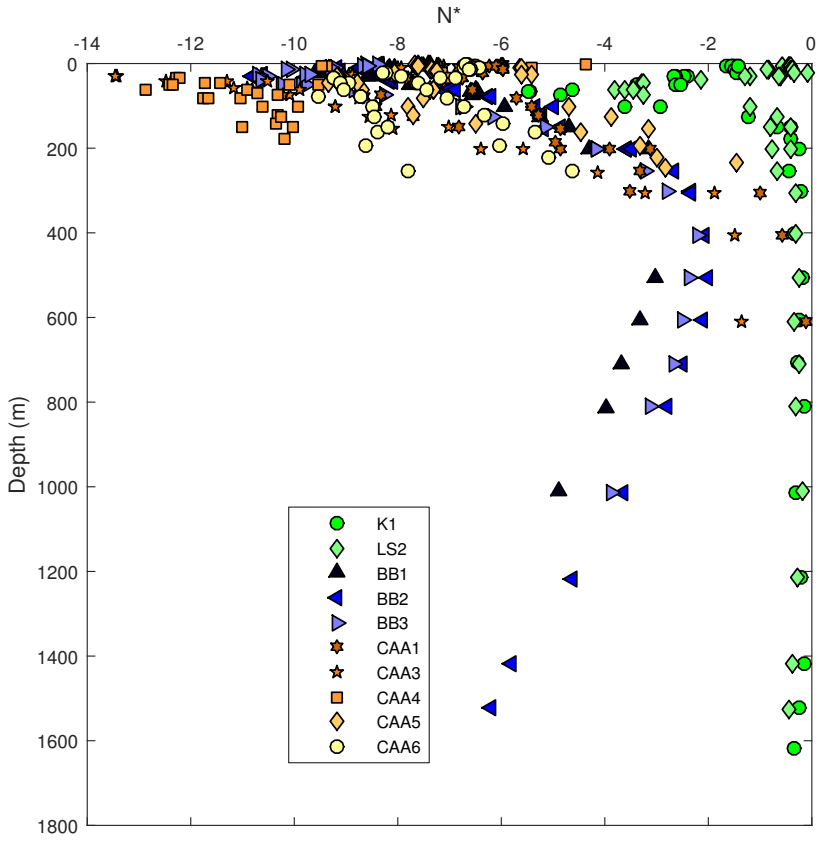


**Figure A.4:** N* for GEOTRACES stations where $\Delta N_2/Ar$ was sampled

had not occurred. In other words, we calculate an initial N* before reductions by denitrification. Figure A.6 shows the profile of $\Delta N_2/Ar$ at station BB3 with the background value from the Labrador Sea. Utilizing the difference between the profile and the background, we calculated the amount of fixed nitrogen that would need to have been removed from the system by denitrification to create the increase in observed $\Delta N_2/Ar$ over the background and added this to the N* profile at BB3. Essentially we are calculating what the source water N* would need to have been to support denitrification causing both the observed $\Delta N_2/Ar$ and N* for this profile. The theoretical starting N* and measured N* profiles for BB3 are shown in Figure A.7. To get the final profiles we observe in the BB, there would need to be source water with N* values of approximately 5. Values of N* this high are essentially isolated to

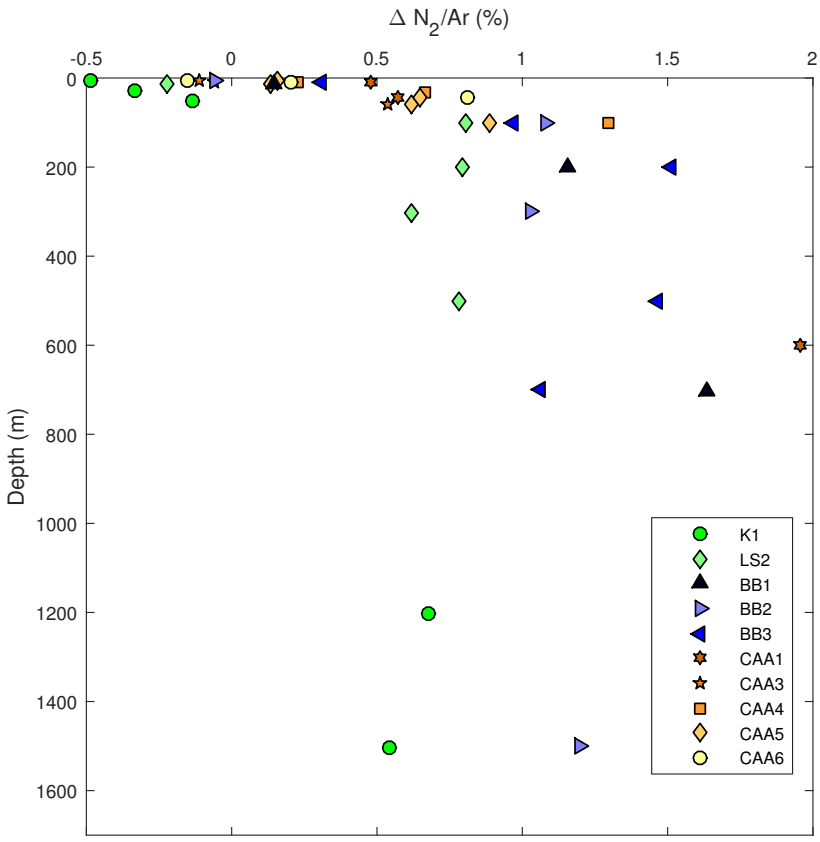


**Figure A.5:** $\Delta N_2/Ar$ from GEOTRACES, average of duplicates with standard deviations less than 0.1

the subtropical North Atlantic thermocline [*Deutsch and Weber*, 2012], an unlikely source water for this region.

We also plotted N* versus $\Delta N_2/Ar$ for all depths (Figure A.8) and only depths greater than 100m (Figure A.9). Baffin Bay and the Labrador Sea have very different relationships between N* and $\Delta N_2/Ar$. Denitrification should cause a $\Delta N_2/Ar$ increase and N* decrease. If anything, in the BB we see increasing $\Delta N_2/Ar$ correlated with increasing N*, opposite the trend caused by likely biological processes.

At this point there appears to be two possibilities for the high $\Delta N_2/Ar$ and complete disconnect between N* and $\Delta N_2/Ar$. The first is that the $\Delta N_2/Ar$ signal has biological origins, possibly related to the high silicate concentrations found in the deep BB which suggest high rates of remineralization in the deep water of the BB

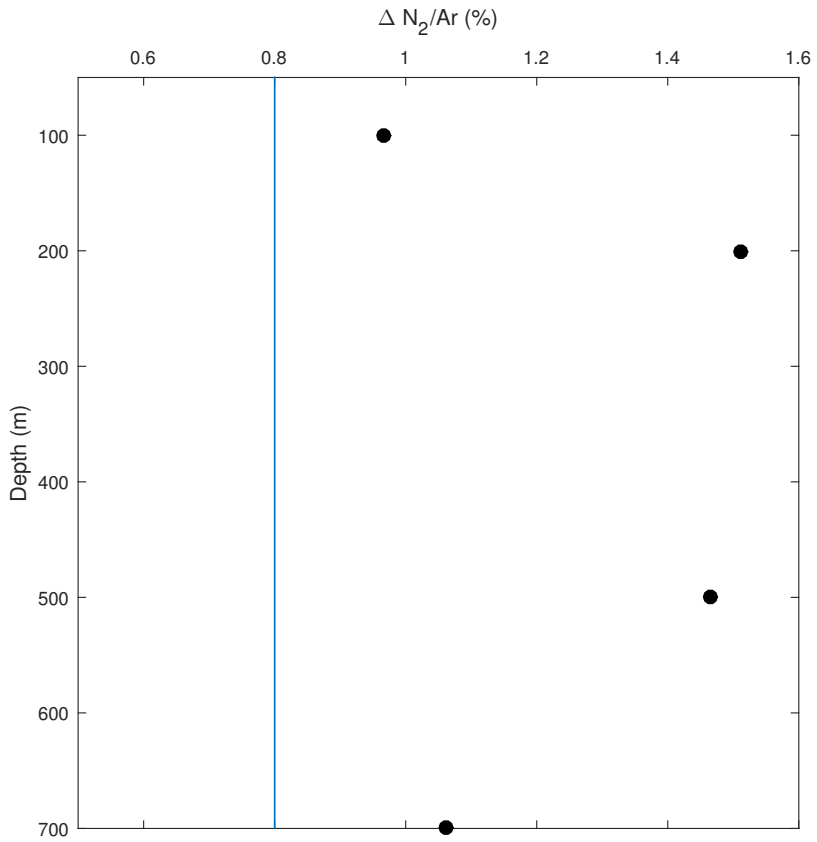


**Figure A.6:** $\Delta N_2/Ar$ versus depth profile for BB3 with the background $\Delta N_2/Ar$ value indicated by the solid blue line

[*Tremblay et al.*, 2002]. If remineralization is high in the deep BB, denitrification rates may also be elevated. The second is that high $\Delta N_2/Ar$ is caused by physical processes involved in the formation of the BB Deep and Bottom waters.

Formation of the Baffin Bay Deep and Bottom waters has been a source of disagreement in the literature [*Bourke et al.*, 1989; *Tremblay et al.*, 2002; *Tang et al.*, 2004]. The two primary hypotheses are subsurface inflow through Nares Strait [*Tang et al.*, 2004] and a mix of Labrador Sea water with brine enriched water from the North Water Polynya [*Bourke et al.*, 1989; *Tang et al.*, 2004]. Due to a lack of measurements of $\Delta N_2/Ar$ in Nares Strait, we cannot support or refute the first theory. The second theory is not supported by our data, given that brine enrichment would likely reduce $\Delta N_2/Ar$ ratios as $N_2$ is preferentially sequestered into bubbles forming

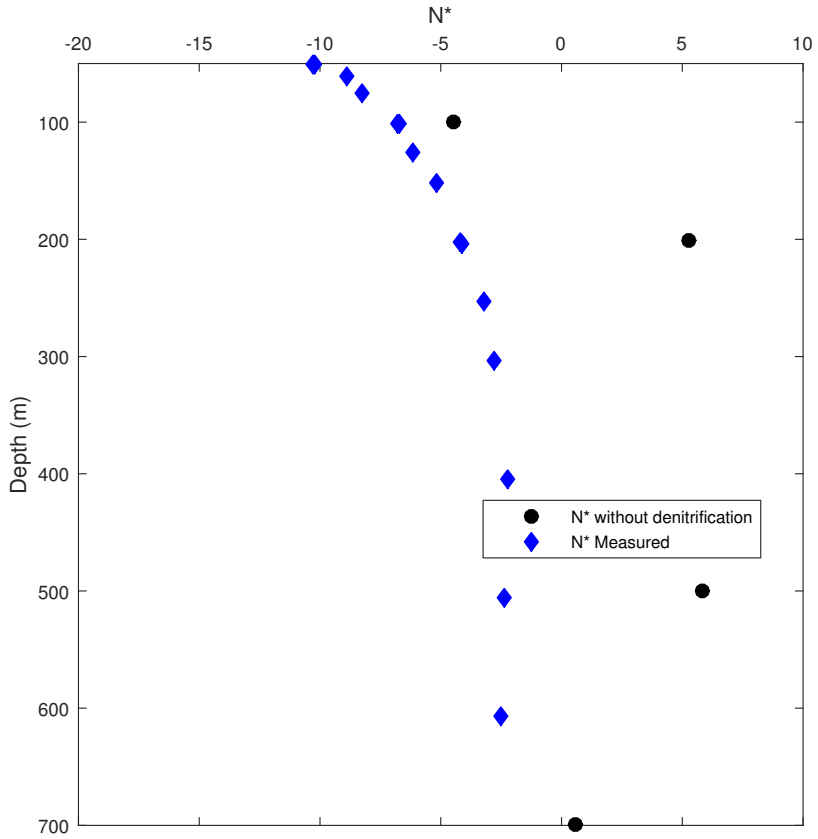


**Figure A.7:** N* versus depth from BB3 and the predicted profile of N* at BB3 if none of the denitrification indicated by $\Delta N_2/Ar$ occurred

in sea ice. *Tremblay et al.* [2002] reports nitrate and silicate remineralization occurring at different depths and concludes that this difference in remineralization depths is primarily driven by biological processes, not physical processes.

To investigate the biological theory, we looked into ratios of N:P and N:Si. The N:P ratio (Figure A.10) shows the BB water transitioning from very nitrate deficient in shallow waters, to more Atlantic type N:P ratios in intermediate layer, before appearing to regain some nitrate deficit in the deepest waters.

The N:Si ratios (Figure A.11) show a clear distinction between the ratio in the deep BB and that of all other water masses.

There is a disconnect between the depths at which remineralization of nitrate and silicate are occurring in BB. Our data, and the data reported by *Tremblay et al.*

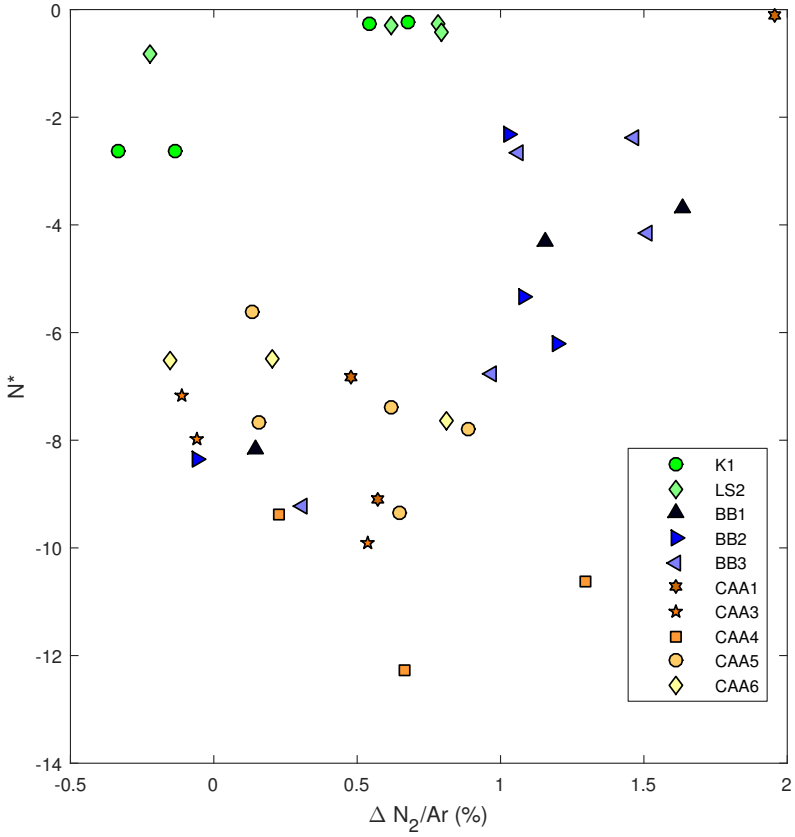


**Figure A.8:** N* versus $\Delta N_2/Ar$ from all depths

[2002], suggest that nitrate is being remineralized in shallow waters, and silicate in deeper waters. *Tremblay et al.* [2002] concluded that this disconnect between the nitrate and silicate remineralizations is driven predominantly by biological processes. Theoretically a process taking up significant amounts of $PO_4$ without consuming $NO_3$ at near Redfield ratios would cause N* to increase, but the BB $PO_4$ profiles (Figure A.12) do not suggest such a process is dominating in the deep BB.

In addition to investigating theories of how these signals could come to exist in BB, we also combed over the $\Delta N_2/Ar$ data which was indicating these signals to determine if there was an issue with the quality control checks we utilize. Figure A.13 shows all of the $\Delta N_2/Ar$ samples measured, without any quality control checks on the agreement of duplicates. One sample is not shown on these plots due to having a value nearly

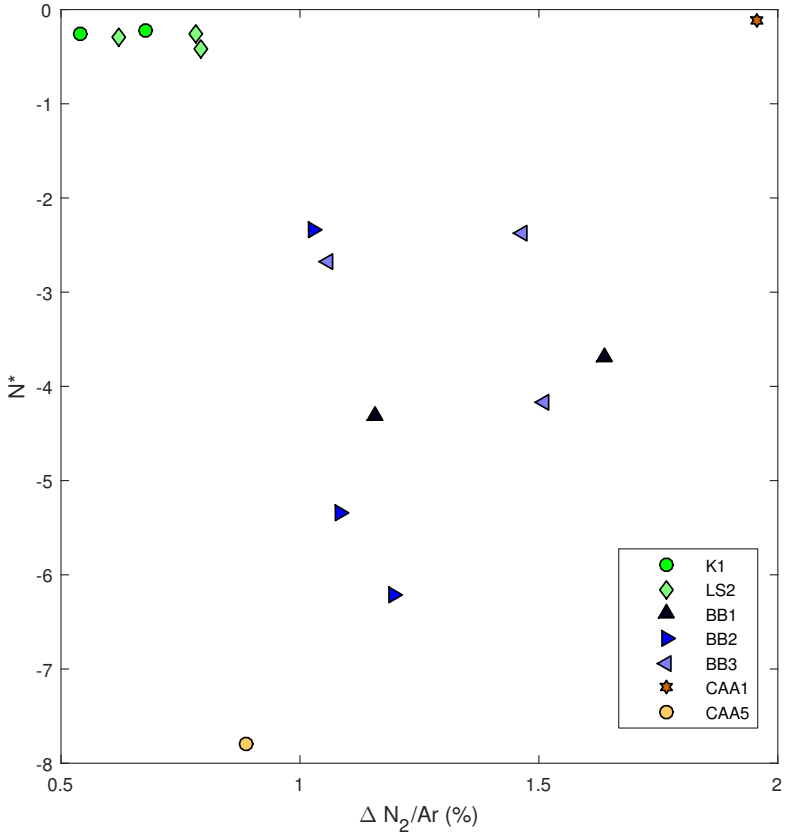


**Figure A.9:** N* versus $\Delta N_2/Ar$ from depths greater than 100 m

double that of all the other samples, and a noted processing error. Figure A.14 shows the standard deviation of duplicates against their averaged $\Delta N_2/Ar$ value. The two lines indicate the two commonly utilized quality control checks on $\Delta N_2/Ar$ duplicates of 0.15, and 0.1 (the check utilized for all data presented in this paper). Higher values of $\Delta N_2/Ar$ are not associated with poorer reproducibility, which suggests that high $\Delta N_2/Ar$ values are not due to air contamination or other analytical problems which should introduce variability.

We additionally checked that there was no relationship between the standard deviation of duplicates and the standards against which they were run. Our lab utilizes two air standards against which all samples are run, VONA1, which has $O_2/N_2/Ar$ ratios similar to surface water, and VONA2, which has half the $O_2$ content

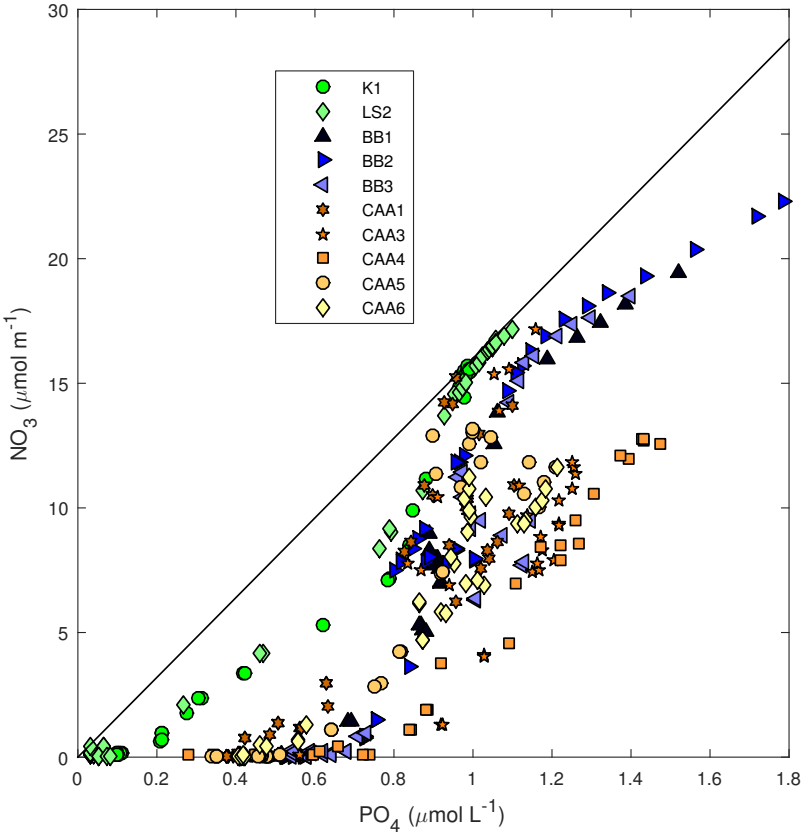


**Figure A.10:** $NO_3$ versus $PO_4$ for GEOTRACES stations where $\Delta N_2/Ar$ was sampled

of VONA1. We run against these two different standards because differences in the $O_2$ content on the sample and standard sides of the dual-inlet mass spectrometer can cause small offsets in the $N_2/Ar$ ratios. We correct for this effect using a series of standards with known $O_2/N_2/Ar$ ratios and varying $O_2$ content. Most samples were run with both dupliates run against VONA1, with some duplicate pairs run one against VONA1 and one against VONA2, and some duplicates were run both against VONA2 (Table A.1). If our chemical slope corrections were inaccurate, we would expect to see larger error when duplicate samples were run against different standards. However, there appears to be no relationship between the standards against which a duplicate pair was run and their standard deviation.

In summary, we don't know why the $\Delta N_2/Ar$ is so high in the BB and so different

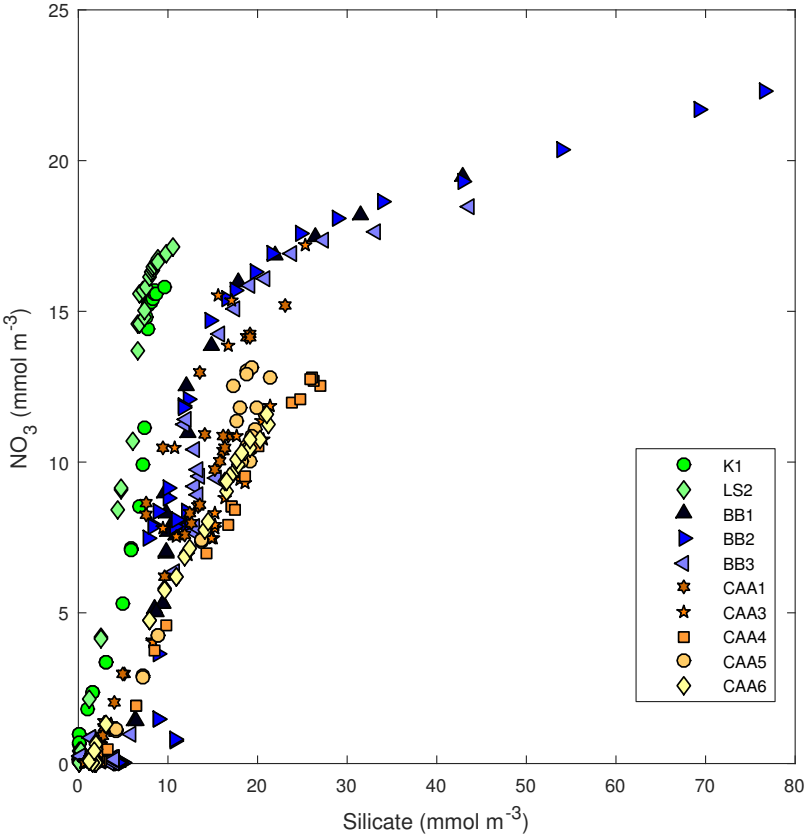


**Figure A.11:** $NO_3$ versus silicate

**Table A.1**

| Standard duplicate run against | Mean (all samples) | Mean (standard deviation¡0.15) | Mean (standard deviation¡0.1) | Minimum standard deviation | Maximum standard deviation |
|---|---|---|---|---|---|
| Both VONA1 | 0.11 (n=46) | 0.049 (n=35) | 0.0593 (n=41) | 0.00 | 2.16 |
| Both VONA2 | 0.12 (n=2) | 0.06 (n=1) | 0.06 (n=1) | 0.06 | 0.18 |
| VONA1 and VONA2 | 0.104 (n=9) | 0.05 (n=4) | 0.081 (n=7) | 0.03 | 0.2 |
| All | 0.1131 (n=57) | 0.0494 (n=40) | 0.0624 (n=49) | 0.00 | 2.16 |

from the expected values given N*. We have conducted initial investigations in the possibility that this difference was due to an analytical problem, the physical formation of the water masses, and biological processes. We have found no evidence in any of these hypotheses which can explain our observations.

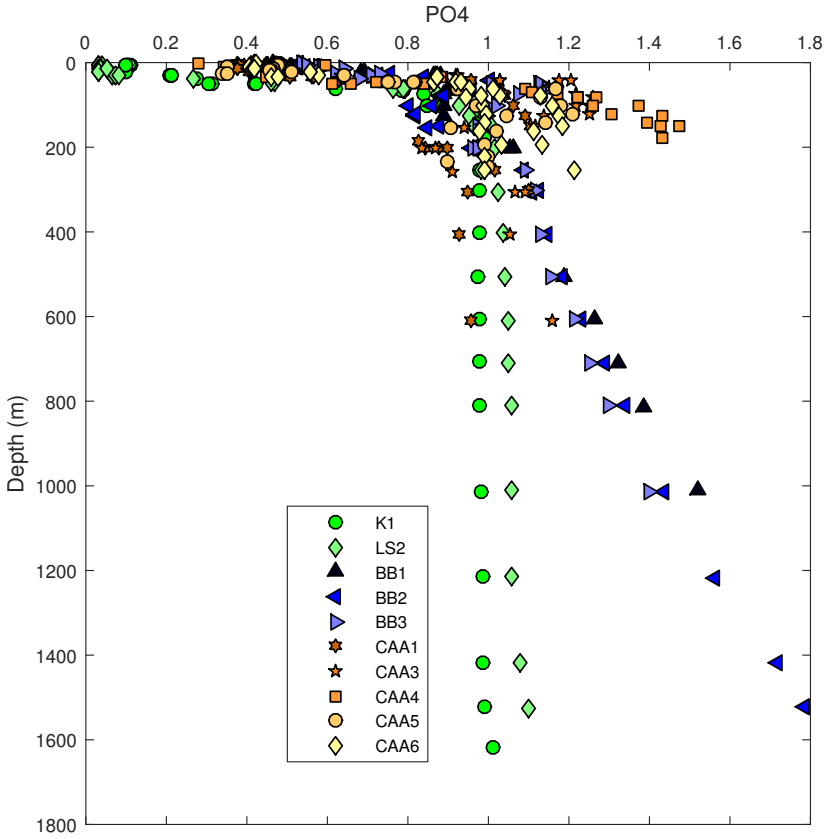


**Figure A.12:** $PO_4$ for GEOTRACES stations where $\Delta N_2/Ar$ was sampled.

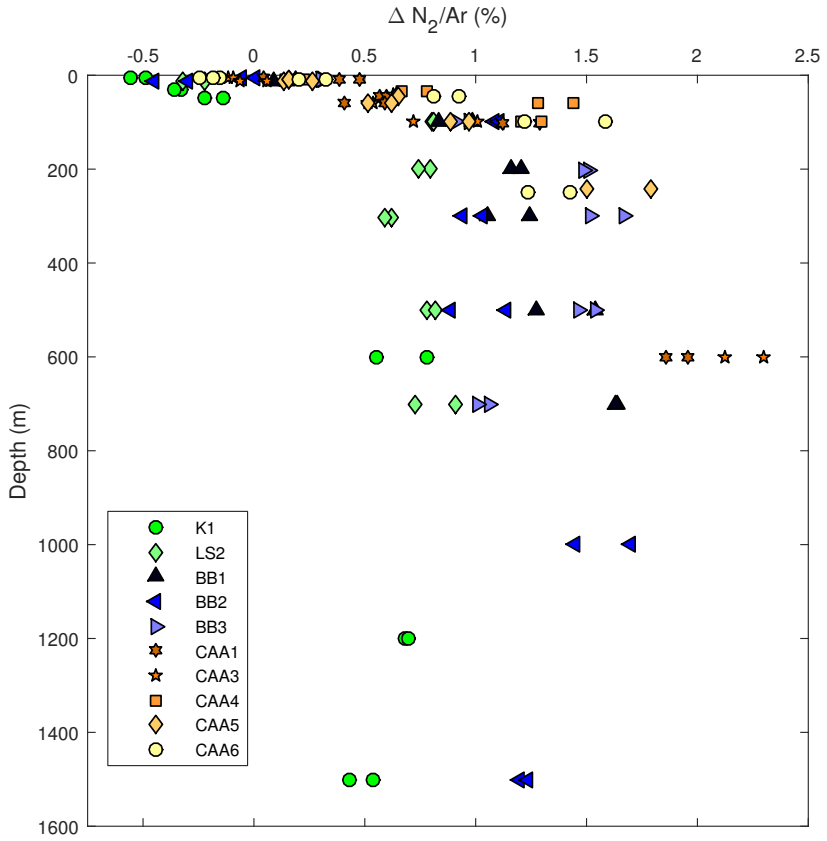


**Figure A.13:** $\Delta N_2/Ar$ measurements from GEOTRACES, duplicates not averaged and no quality control

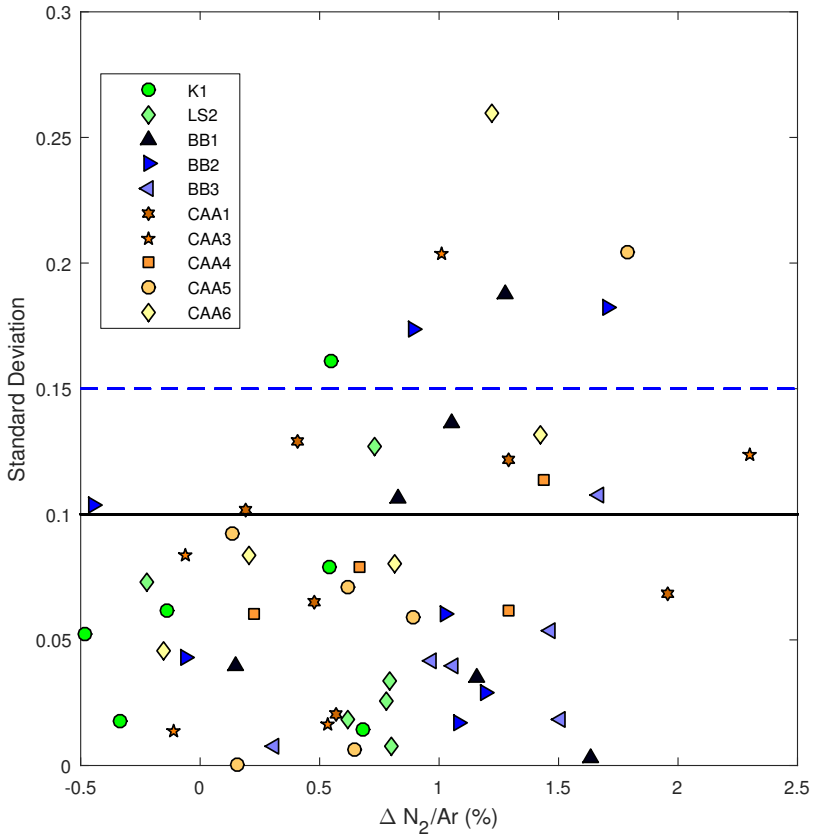


**Figure A.14:** $\Delta N_2/Ar$ versus standard deviation of duplicates. The solid black line indicates a quality control of standard deviations less than 0.1, the dashed blue line is a standard deviation of 0.15. One set of duplicates is not shown here as its standard deviation is greater than 2.

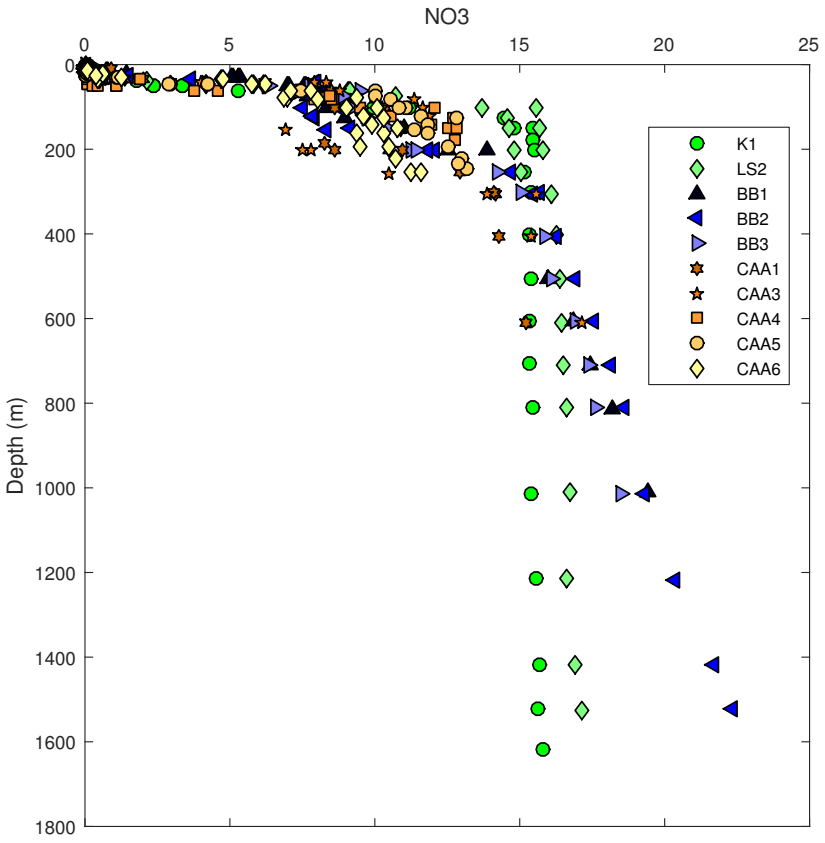


**Figure A.15:** $NO_3$ for GEOTRACES stations where $\Delta N_2/Ar$ was sampled

# Bibliography

Altabet, A., D. W. Murray, and W. L. Prell, Climatically linked oscillations in Arabian Sea denitrification over the past 1 m.y.: Implications for the marine N cycle, *Paleoceanography*, *14*(6), 732–743, 1999.

Altabet, M. a., M. J. Higginson, and D. W. Murray, The effect of millennial-scale changes in Arabian Sea denitrification on atmospheric CO2., *Nature*, *415*(6868), 159–162, doi:10.1038/415159a, 2002.

Anderson, L. G., P. S. Andersson, G. Björk, E. P. Jones, S. Jutterström, and I. Wåhlstrom, Source and formation of the upper halocline of the Arctic Ocean, *Journal of Geophysical Research: Oceans*, *118*(1), 410–421, doi:10.1029/2012JC008291, 2013.

Bianchi, D., J. P. Dunne, J. L. Sarmiento, and E. D. Galbraith, Data-based estimates of suboxia, denitrification, and N2O production in the ocean and their sensitivities to dissolved O2, *Global Biogeochem. Cycles*, *26*(2), doi:10.1029/2011gb004209, 2012.

Blais, M., J.-É. Tremblay, A. D. Jungblut, J. Gagnon, J. Martin, M. Thaler, and C. Lovejoy, Nitrogen fixation and identification of potential diazotrophs in the Canadian Arctic, *Global Biogeochemical Cycles*, *26*, doi:10.1029/2011GB004096, 2012.

Bourbonnais, A., M. A. Altabet, C. N. Charoenpong, J. Larkum, H. Hu, H. W. Bange, and L. Stramma, N-loss isotope effect in the Peru oxygen minimum zone studied using a mesoscale eddy as a natural tracer experiment, *Global Biogeochemical Cycles*, *29*, 793–811, doi:10.1002/2014GB005001.Received, 2015.

Bourke, R. H., V. G. Addison, and R. G. Paquette, Oceanography of Nares Strait and northern Baffin Bay in 1986 with emphasis on deep and bottom water formation, *Journal of Geophysical Research*, *94*(C6), 8289, doi:10.1029/JC094iC06p08289, 1989.

Brown, Z. W., K. L. Casciotti, R. S. Pickart, J. H. Swift, and K. R. Arrigo, Aspects of the marine nitrogen cycle of the Chukchi Sea shelf and Canada Basin, *Deep-Sea Research Part II: Topical Studies in Oceanography*, *118*, 73–87, doi:10.1016/j.dsr2.2015.02.009, 2015.

Carmack, E. C., W. J. Williams, S. L. Zimmermann, and F. A. McLaughlin, The Arctic Ocean warms from below, *Geophysical Research Letters*, *39*(April), 1–6, doi:10.1029/2012GL050890, 2012.

Chang, B. X., and A. H. Devol, Seasonal and spatial patterns of sedimentary denitrification rates in the Chukchi sea, *Deep-Sea Research Part II: Topical Studies in Oceanography*, *56*(17), 1339–1350, doi:10.1016/j.dsr2.2008.10.024, 2009.

Chang, B. X., A. H. Devol, and S. R. Emerson, Denitrification and the nitrogen gas excess in the eastern tropical South Pacific oxygen deficient zone, *Deep-Sea Research Part I: Oceanographic Research Papers*, *57*(9), 1092–1101, doi:10.1016/j.dsr.2010.05.009, 2010.

Chang, B. X., A. H. Devo, and S. R. Emerson, Fixed nitrogen loss from the eastern tropical North Pacific and Arabian Sea oxygen deficient zones determined

from measurements of N2:Ar, *Global Biogeochemical Cycles*, *26*(3), 1–8, doi: 10.1029/2011GB004207, 2012.

Chu, P. C., Q. Q. Wang, and R. H. Bourke, A geometric model for the Beaufort Chukchi Sea thermohaline structure, *Journal of Atmospheric and Oceanic Technology*, *16*(6), 613–632, 1999.

Codispoti, L., and J. Christensen, Nitrification, denitrification and nitrous oxide cycling in the eastern tropical South Pacific ocean, *Marine Chemistry*, *16*(4), 277–300, doi:10.1016/0304-4203(85)90051-9, 1985.

Codispoti, L. A., An oceanic fixed nitrogen sink exceeding 400 Tg N a$ˆ{-1}$ vs the concept of homeostasis in the fixed-nitrogen inventory, *Biogeosciences*, *4*, 233–253, doi:10.5194/bgd-3-1203-2006, 2007.

Codispoti, L. A., C. Flagg, V. Kelly, and J. H. Swift, Hydrographic conditions during the 2002 SBI process experiments, *Deep Sea Research II*, *52*, 3199–3226, doi: 10.1016/j.dsr2.2005.10.007, 2005.

Codispoti, L. A., C. N. Flagg, and J. H. Swift, Hydrographic conditions during the 2004 SBI process experiments, *Deep Sea Research II*, *56*, 1144–1163, doi: 10.1016/j.dsr2.2008.10.013, 2009.

Comiso, J. C., and C. L. Parkinson, Arctic sea ice parameters from AMSR-E data using two techniques and comparisons with sea ice from SSM/I, *Journal of Geophysical Research: Oceans*, *113*(2), 1–16, doi:10.1029/2007JC004255, 2008.

Cooper, L. W., T. E. Whitledge, J. M. Grebmeier, and T. Weingartner, The nutrient, salinity, and stable oxygen isotope composition of Bering and Chukchi Seas waters in and near the Bering Strait, *102*(C6), 12,563–12,573, 1997.

Curry, B., C. M. Lee, and B. Petrie, Volume, Freshwater, and Heat Fluxes through Davis Strait, 200405*, *Journal of Physical Oceanography*, *41*(3), 429–436, doi: 10.1175/2010JPO4536.1, 2011.

Deutsch, C., and T. Weber, Nutrient Ratios as a Tracer and Driver of Ocean Biogeochemistry, *Annual Review of Marine Science*, *4*(1), 113–141, doi:10.1146/annurev-marine-120709-142821, 2012.

Devol, A. H., L. A. Codispoti, and J. P. Christensen, Summer and winter denitrification rates in western Arctic shelf sediments, *Continental Shelf Research*, *17*(9), 1029–1050, doi:Doi 10.1016/S0278-4343(97)00003-4, 1997.

DeVries, T., C. Deutsch, P. A. Rafter, and F. Primeau, Marine denitrification rates determined from a global 3-D inverse model, *Biogeosciences*, *10*(4), 2481–2496, doi:10.5194/bg-10-2481-2013, 2013.

Emerson, S., C. Stump, D. Wilbur, and P. Quay, Accurate measurement of O_2, N_2, and Ar gases in water and the solubility of N_2, *Marine Chemistry*, *64*(4), 337–347, doi:10.1016/S0304-4203(98)00090-5, 1999.

Engstrom, P., C. R. Penton, and A. H. Devol, Anaerobic ammonium oxidation in deep-sea sediments off the Washington margin, *Limnology and Oceanography*, *54*(5), 1643–1652, doi:10.4319/lo.2009.54.5.1643, 2009.

Galbraith, E. D., et al., The acceleration of oceanic denitrification during deglacial warming, *Nature Geoscience*, *6*(7), 579–584, doi:10.1038/ngeo1832, 2013.

Granger, J., M. G. Prokopenko, D. M. Sigman, C. W. Mordy, Z. M. Morse, L. V. Morales, R. N. Sambrotto, and B. Plessen, Coupled nitrification-denitrification in sediment of the eastern Bering Sea shelf leads to $ˆ{15}$N enrichment of fixed

N in shelf waters, *Journal of Geophysical Research: Oceans*, *116*(11), 1–18, doi: 10.1029/2010JC006751, 2011.

Grebmeier, J. M., S. E. Moore, J. E. Overland, K. E. Frey, and R. Gradinger, Biological Response to Recent Pacific Arctic Sea Ice Retreats, *EOS*, *91*(18), 161–162, doi:10.1029/2010EO180001, 2010.

Gruber, N., The Dynamics of the Marine Nitrogen Cycle and its Influence on Atmospheric CO$_2$ Variations, *The Ocean Carbon Cycle and Climate*, *40*, 97–148, 2004.

Gruber, N., and J. L. Sarmiento, Global patterns of marine nitrogen fixation and denitrification, *Global Biogeochemical Cycles*, *11*(2), 235, doi:10.1029/97GB00077, 1997.

Hamme, R. C., and S. R. Emerson, Mechanisms controlling the global oceanic distribution of the inert gases argon, nitrogen and neon, *Geophysical Research Letters*, *29*(23), 2120, doi:10.1029/2002GL015273, 2002.

Hamme, R. C., and S. R. Emerson, The solubility of neon, nitrogen and argon in distilled water and seawater, *Deep-Sea Research Part I: Oceanographic Research Papers*, *51*(11), 1517–1528, doi:10.1016/j.dsr.2004.06.009, 2004.

Hamme, R. C., and S. R. Emerson, Deep-sea nutrient loss inferred from the marine dissolved $N_2$/Ar ratio, *Geophysical Research Letters*, *40*(6), 1149–1153, doi: 10.1002/grl.50275, 2013.

Hamme, R. C., S. R. Emerson, J. P. Severinghaus, and M. C. Long, Using noble gas measurements to derive air-sea process information and predict physical gas saturations, *Geophysical Research Letters*, 2017.

Ho, D. T., C. S. Law, M. J. Smith, P. Schlosser, M. Harvey, and P. Hill, Measurements of air-sea gas exchange at high wind speeds in the Southern Ocean: Implications for global parameterizations, *Geophysical Research Letters*, *33*(16), 1–6, doi:10.1029/2006GL026817, 2006.

Ingall, E., and R. Jahnke, Evidence for enhanced phosphorus regeneration from marine sediments overlain by oxygen depleted waters, *Geochimica et Cosmochimica Acta*, *58*(11), 2571–2575, doi:10.1016/0016-7037(94)90033-7, 1994.

Ito, M., Y. W. Watanabe, M. Shigemitsu, S. S. Tanaka, and J. Nishioka, Application of chemical tracers to an estimate of benthic denitrification in the Okhotsk Sea, *Journal of Oceanography*, *70*(5), 415–424, doi:10.1007/s10872-014-0241-9, 2014.

Itoh, M., K. Shimada, T. Kamoshida, F. McLaughlin, E. Carmack, and S. Nishino, Interannual variability of Pacific Winter Water inflow through Barrow Canyon from 2000 to 2006, *Journal of Oceanography*, *68*(4), 575–592, doi:10.1007/s10872-012-0120-1, 2012.

Jones, E. P., J. H. Swift, L. G. Anderson, M. Lipizer, G. Civitarese, K. K. Falkner, G. Kattner, and F. McLaughlin, Tracing Pacific water in the North Atlantic Ocean, *Journal of Geophysical Research*, *108*(C4), 3116, doi:10.1029/2001JC001141, 2003.

Kawaguchi, Y., S. Nishino, and J. Inoue, Fixed-Point Observation of Mixed Layer Evolution in the Seasonally Ice-Free Chukchi Sea: Turbulent Mixing due to Gale Winds and Internal Gravity Waves., *Journal of Physical Oceanography*, *45*(3), 836–853, doi:10.1175/JPO-D-14-0149.1, 2015.

Kirtman, B., et al., Near-term Climate Change: Projections and Predictability, in *Climate Change 2013: The Physical Science Basis. Contribution of Working Group I to the Fifth Assessment Report of the Intergovernmental Panel on Climate Change*,

edited by T. Stocker, D. Qin, G.-K. Plattner, M. Tignor, S. Allen, J. Boschung, A. Nauels, Y. Xia, V. Bex, and P. Midgley, pp. 953–1028, Cambridge University Press, doi:10.1017/CBO9781107415324.023, 2013.

Larsen, J., O. Anisimov, A. Constable, A. Holloweed, N. Maynard, P. Prestrud, T. Prowse, and J. Stone, Polar Regions, in *Climate Change 2014: Impacts, Adaptation, and Vulnerability. Part B: Regional Aspects. Contribution of Working Group II to the Fifth Assessment Report of the Intergovernmental Panel on Climate Change*, edited by V. Barros, C. Field, D. Dokken, M. Mastrandrea, K. Mach, T. Bilir, M. Chatterjee, K. Ebi, Y. Estrada, R. Genova, B. Girma, E. Kissel, A. Levy, S. MacCracken, P. Mastrandrea, and L. White, pp. 1567–1612, Cambridge University Press, 2014.

Liu, Z., M. A. Altabet, and T. D. Herbert, Glacial-interglacial modulation of eastern tropical North Pacific denitrification over the last 1.8-Myr, *Geophysical Research Letters*, *32*(23), 1–4, doi:10.1029/2005GL024439, 2005.

Macdonald, R. W., and E. C. Carmack, Age of Canada Basin Deep Waters: A Way to Estimate Primary Producition for the Arctic Ocean, *Science*, *254*(5036), 1348–1350, 1991.

Macdonald, R. W., and E. C. Carmack, Tritium and Radiocarbon Dating of Canada Basin Deep Waters, *Science*, *259*(5091), 103–104, 1993.

Macdonald, R. W., E. Sakshaug, and R. Stein, The Arctic Ocean: Modern Status and Recent Climate Change, in *The Organic Carbon Cycle in the Arctic Ocean*, edited by R. Stein and R. W. Macdonald, chap. 2, pp. 6–20, Springer, 2004.

Manning, C. C., R. C. Hamme, and A. Bourbonnais, Impact of deep-water renewal

events on fixed nitrogen loss from seasonally-anoxic Saanich Inlet, *Marine Chemistry*, *122*(1-4), 1–10, doi:10.1016/j.marchem.2010.08.002, 2010.

Manucharyan, G. E., M. A. Spall, A. F. Thompson, G. E. Manucharyan, M. A. Spall, and A. F. Thompson, A Theory of the Wind-Driven Beaufort Gyre Variability, *Journal of Physical Oceanography*, *46*(11), 3263–3278, doi:10.1175/JPO-D-16-0091.1, 2016.

Martin, W. R., and F. L. Sayles, Organic matter cycling in sediments of the continental margin in the northwest Atlantic Ocean, *Deep-Sea Research Part I: Oceanographic Research Papers*, *51*(3), 457–489, doi:10.1016/j.dsr.2003.10.013, 2004.

McElroy, M. B., Marine biological controls on atmospheric CO2 and climate, doi:10.1038/302328a0, 1983.

McLaughlin, F. A., E. C. Carmack, R. W. Macdonald, H. Melling, J. H. Swift, P. A. Wheeler, B. F. Sherr, and E. B. Sherr, The joint roles of Pacific and Atlantic-origin waters in the Canada Basin, 1997-1998, *Deep-Sea Research Part I: Oceanographic Research Papers*, *51*(1), 107–128, doi:10.1016/j.dsr.2003.09.010, 2004.

McTigue, N. D., W. S. Gardner, K. H. Dunton, and A. K. Hardison, Biotic and abiotic controls on co-occurring nitrogen cycling processes in shallow Arctic shelf sediments, *Nature Communications*, *7*, 13,145, doi:10.1038/ncomms13145, 2016.

Middelburg, J. J., K. Soetaert, P. M. J. Herman, and C. H. R. Heip, Denitrification in marine sediments: A model study, *Global Biogeochemical Cycles*, *10*(4), 661–673, 1996.

Mills, M. M., et al., Impacts of low phytoplankton NO$_3$ utilization ratios over the Chukchi Shelf , Arctic Ocean, *Deep-Sea Research Part II*, *118*, 105–121, doi:10.1016/j.dsr2.2015.02.007, 2015.

Newton, R., P. Schlosser, R. Mortlock, J. Swift, and R. MacDonald, Canadian Basin freshwater sources and changes: Results from the 2005 Arctic Ocean Section, *Journal of Geophysical Research: Oceans*, *118*(4), 2133–2154, doi:10.1002/jgrc.20101, 2013.

Nishino, S., K. Shimada, and M. Itoh, Use of ammonium and other nitrogen tracers to investigate the spreading of shelf waters in the western Arctic halocline, *Journal of Geophysical Research*, *110*(C10005), 1–6, doi:10.1029/2003JC002118, 2005.

Nishino, S., K. Shimada, M. Itoh, M. Yamamoto-Kawai, and S. Chiba, East-west differences in water mass, nutrient, and chlorophyll a distributions in the sea ice reduction region of the western Arctic Ocean, *Journal of Geophysical Research*, *113*, C00A01, doi:10.1029/2007JC004666, 2008.

Nishino, S., Y. Kawaguchi, J. Inoue, T. Hirawake, A. Fujiwara, R. Futsuki, J. Onodera, and M. Aoyama, Nutrient supply and biological response to wind-induced mixing, inertial motion, internal waves, and currents in the northern Chukchi Sea, *Journal of Geophysical Research C: Oceans*, *120*(3), 1975–1992, doi:10.1002/2014JC010407, 2015.

Paytan, A., and K. McLaughlin, The oceanic phosphorus cycle, *Chemical Reviews*, *107*(2), 563–576, doi:10.1021/cr0503613, 2007.

Pickart, R. S., T. J. Weingartner, L. J. Pratt, S. Zimmermann, and D. J. Torres, Flow of winter-transformed Pacific water into the Western Arctic, *Deep-Sea Research Part II: Topical Studies in Oceanography*, *52*(24-26), 3175–3198, doi:10.1016/j.dsr2.2005.10.009, 2005.

Piper, M. M., C. R. Benitez-Nelson, K. E. Frey, M. M. Mills, and S. Pal, Dissolved and particulate phosphorus distributions and elemental stoichiometry throughout

the Chukchi Sea, *Deep Sea Research Part II: Topical Studies in Oceanography*, *130*, 76–87, doi:http://dx.doi.org/10.1016/j.dsr2.2016.05.009, 2016.

Rudels, B., Arctic ocean circulation, in *Encyclopedia of Ocean Sciences*, pp. 211–225, 2009.

Rudels, B., Arctic Ocean circulation, processes and water masses: A description of observations and ideas with focus on the period prior to the International Polar Year 2007-2009, *Progress in Oceanography*, *132*, 22–67, doi:10.1016/j.pocean.2013.11.006, 2015.

Schlosser, P., B. Kromer, B. Ekwurzel, G. Bonisch, A. McNichol, R. Schneider, K. von Reden, H. Ostlund, and J. H. Swift, The first trans-Arctic $ˆ{14}$C section : comparison of the mean ages of the deep waters in the Eurasian and Canadian basins of the Arctic Ocean, *Nuclear Instruments and Methods in Physics Research B*, *23*(96), 431–437, 1997.

Shigemitsu, M., N. Gruber, A. Oka, and Y. Yamanaka, Potential use of the N2/Ar ratio as a constraint on the oceanic fixed nitrogen loss, *Global Biogeochemical Cycles*, *30*, 576–594, doi:10.1002/2015GB005129.Received, 2016.

Simpson, K. G., J.-É. Tremblay, Y. Gratton, and N. M. Price, An annual study of inorganic and organic nitrogen and phosphorus and silicic acid in the southeastern Beaufort Sea, *Journal of Geophysical Research*, *113*, 1–16, doi:10.1029/2007JC004462, 2008.

Souza, A. C., I.-n. Kim, W. S. Gardner, and K. H. Dunton, Dinitrogen, oxygen, and nutrient fluxes at the sediment-water interface and bottom water physical mixing on the eastern Chukchi Sea shelf, *Deep-Sea Research Part II*, *102*, 77–83, doi:10.1016/j.dsr2.2014.01.002, 2014.

Stegall, S. T., and J. Zhang, Wind field climatology, changes, and extremes in the Chukchi-Beaufort seas and Alaska north slope during 1979-2009, *Journal of Climate*, *25*(23), 8075–8089, doi:10.1175/JCLI-D-11-00532.1, 2012.

Steiner, N., Trends and projections of acidification and primary production in the Canadian Arctic, *Canadian Meteorological and Oceanographic Society Bulletin*, *43*(6), 187–192, 2015.

Tanaka, T., L. Guo, C. Deal, N. Tanaka, T. Whitledge, and A. Murata, N deficiency in a well-oxygenated cold bottom water over the Bering Sea shelf: Influence of sedimentary denitrification, *Continental Shelf Research*, *24*(12), 1271–1283, doi: 10.1016/j.csr.2004.04.004, 2004.

Tang, C. C. L., C. K. Ross, T. Yao, B. Petrie, B. M. DeTracey, and E. Dunlap, The circulation, water masses and sea-ice of Baffin Bay, *Progress in Oceanography*, *63*(4), 183–228, doi:10.1016/j.pocean.2004.09.005, 2004.

Timmermans, M.-L., and C. Garrett, Evolution of the Deep Water in the Canadian Basin in the Arctic Ocean, *Journal of Physical Oceanography*, *36*(5), 866–874, doi: 10.1175/JPO2906.1, 2006.

Timmermans, M.-l., C. Garrett, and E. Carmack, The thermohaline structure and evolution of the deep waters in the Canada Basin, Arctic Ocean, *Deep-Sea Research Part I*, *50*, 1305–1321, doi:10.1016/S0967-0637(03)00125-0, 2003.

Timmermans, M. L., et al., Mechanisms of Pacific Summer Water variability in the Arctic's Central Canada Basin, *Journal of Geophysical Research C: Oceans*, *119*(11), 7523–7548, doi:10.1002/2014JC010273, 2014.

Tremblay, J.-É., Y. Gratton, E. C. Carmack, C. D. Payne, and N. M. Price, Impact of the large-scale Arctic circulation and the North Water Polynya on nutrient

inventories in Baffin Bay, *Journal of Geophysical Research*, *107*(C8), 1–15, doi: 10.1029/2000JC000595, 2002.

Tremblay, J.-É., et al., Current state and trends in Canadian Arctic marine ecosystems: I. Primary production, *Climatic Change*, *115*, 161–178, doi:10.1007/s10584-012-0496-3, 2012.

Trimmer, M., and J. C. Nicholls, Production of nitrogen gas via anammox and denitrification in intact sediment cores along a continental shelf to slope transect in the North Atlantic, *Limnology and Oceanography*, *54*(2), 577–589, doi: 10.4319/lo.2009.54.2.0577, 2009.

Vaughan, D., et al., Observations: Cryosphere, *Climate Change 2013: The Physical Science Basis. Contribution of Working Group I to the Fifth Assessment Report of the Intergovernmental Panel on Climate Change*, pp. 317–382, doi: 10.1017/CBO9781107415324.012, 2013.

Weber, T. S., and C. Deutsch, Ocean nutrient ratios governed by plankton biogeography., *Nature*, *467*(7315), 550–554, doi:10.1038/nature09403, 2010.

Weingartner, T., E. Dobbins, S. Danielson, P. Winsor, R. Potter, and H. Statscewich, Hydrographic variability over the northeastern Chukchi Sea shelf in summer-fall 2008-2010, *Continental Shelf Research*, *67*, 5–22, doi:10.1016/j.csr.2013.03.012, 2013.

Whitney, F. A., and H. J. Freeland, Variability in upper-ocean water properties in the NE Pacific Ocean, *Deep-Sea Research Part II*, *46*, 2351–2370, 1999.

Yamamoto-Kawai, M., E. Carmack, and F. McLaughlin, Nitrogen balance and Arctic throughflow., *Nature*, *443*(7107), 43, doi:10.1038/443043a, 2006.

Zhong, W., and J. Zhao, Deepening of the Atlantic Water Core in the Canada Basin in 2003-11, *Journal of Physical Oceanography*, *44*(9), 2353–2369, doi:10.1175/JPO-D-13-084.1, 2014.